

## Redox-Active 1D Coordination Polymers of Iron-Sulfur Clusters

Noah E. Horwitz, Jiaze Xie, Alexander S. Filatov, Robert J. Papoular, William E. Shepard, David Z. Zee, Mia P. Grahn, Chloe Gilder, and John S. Anderson

*J. Am. Chem. Soc.*, **Just Accepted Manuscript** • DOI: 10.1021/jacs.8b12339 • Publication Date (Web): 04 Feb 2019

Downloaded from <http://pubs.acs.org> on February 4, 2019

### Just Accepted

“Just Accepted” manuscripts have been peer-reviewed and accepted for publication. They are posted online prior to technical editing, formatting for publication and author proofing. The American Chemical Society provides “Just Accepted” as a service to the research community to expedite the dissemination of scientific material as soon as possible after acceptance. “Just Accepted” manuscripts appear in full in PDF format accompanied by an HTML abstract. “Just Accepted” manuscripts have been fully peer reviewed, but should not be considered the official version of record. They are citable by the Digital Object Identifier (DOI®). “Just Accepted” is an optional service offered to authors. Therefore, the “Just Accepted” Web site may not include all articles that will be published in the journal. After a manuscript is technically edited and formatted, it will be removed from the “Just Accepted” Web site and published as an ASAP article. Note that technical editing may introduce minor changes to the manuscript text and/or graphics which could affect content, and all legal disclaimers and ethical guidelines that apply to the journal pertain. ACS cannot be held responsible for errors or consequences arising from the use of information contained in these “Just Accepted” manuscripts.



# Redox-Active 1D Coordination Polymers of Iron-Sulfur Clusters

Noah E. Horwitz,<sup>†‡</sup> Jiaze Xie,<sup>†‡</sup> Alexander S. Filatov,<sup>†</sup> Robert J. Papoular,<sup>§</sup> William E. Shepard,<sup>‡</sup> David Z. Zee,<sup>||</sup> Mia P. Grahn,<sup>†</sup> Chloe Gilder,<sup>†</sup> and John S. Anderson<sup>\*†</sup>

<sup>†</sup>Department of Chemistry, University of Chicago, Chicago, Illinois 60637, United States

<sup>§</sup>Saclay Institute for Matter and Radiation [ IRAMIS ], Leon Brillouin Laboratory, CEA-Saclay, 91191 Gif-sur-Yvette, France.

<sup>‡</sup>Synchrotron SOLEIL, L'Orme des Merisiers Saint-Aubin, BP 48, 91192 Gif-sur-Yvette CEDEX, France

<sup>||</sup>Department of Chemistry, Northwestern University, Evanston, Illinois 60208, United States

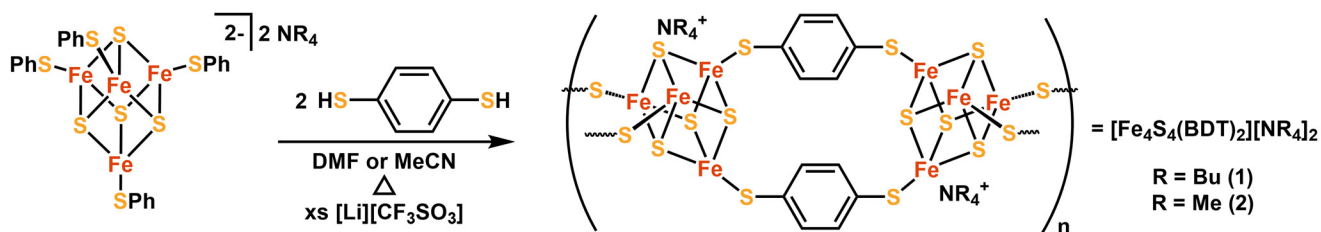
**ABSTRACT:** Here we describe the combination of an archetypal redox-active metal sulfide cluster, Fe<sub>4</sub>S<sub>4</sub>, with an organic linker, 1,4-benzenedithiolate, to prepare coordination polymers containing infinite chains of Fe<sub>4</sub>S<sub>4</sub> clusters. The crystal structures of two solid materials have been solved from synchrotron X-ray powder diffraction data using simulated annealing and refined by a least-squares Rietveld refinement procedure. The electronic properties of these chains have also been characterized by UV-visible and Mössbauer spectroscopies. Additional experiments demonstrated that these chains can be solubilized by variation of the countercation and that the chain structure is maintained in solution. The redox-activity of the Fe<sub>4</sub>S<sub>4</sub> clusters can be accessed with chemical reagents. Introduction of charge carriers by reduction of the Fe<sub>4</sub>S<sub>4</sub> clusters is found to increase the electrical conductivity of the materials by up to four orders of magnitude. These results highlight the utility of Fe<sub>4</sub>S<sub>4</sub> clusters as redox-active building blocks in preparing new classes of coordination polymers.

## INTRODUCTION

Hybrid inorganic-organic materials are an attractive area of research as they can exhibit a wide array of physical and chemical properties that can be tuned through substitution of their components. Recent interest in these types of materials is exemplified by coordination polymers such as metal-organic frameworks (MOFs)<sup>1</sup> and hybrid perovskites.<sup>2</sup> In particular, there has been a surge of interest in coordination polymers exhibiting intrinsic magnetic and conductive properties as these materials show potential for applications in energy storage and electronics.<sup>3</sup> It is crucial to carefully match the properties, particularly the electronic properties, of the metal and linker in these materials to optimize their performance. Detailed studies have shown that moving from O-based linkers to less electronegative and consequently more donating N-based linkers improves coupling and delocalization.<sup>3</sup> By the same rationale, further work has shown that using heavier chalcogenide-based linkers (S-based in particular) in place of more common O- or N-based ligands can enhance electronic coupling leading to improvement in conductivity.<sup>4</sup>

These studies have generated several examples of materials which highlight that the combination of organosulfur ligands with transition metal ions leads to coordination polymers with desirable properties such as high electrical conductivity.<sup>5,6</sup> The

majority of these materials, however, are based on monometallic nodes. Comparatively, the use of metal-chalcogenide clusters as building blocks has been underexplored. The use of metal-chalcogenide clusters to rationally impart desired properties to materials is well demonstrated by recent work in which hydrogen evolution catalysts can be prepared from Mo-S clusters linked by organosulfur ligands.<sup>7</sup> Among possible metal chalcogenide clusters, the cubane-type Fe<sub>4</sub>S<sub>4</sub> cluster stands out as an attractive building block due to its redox-activity, stability, electronic delocalization, and complex magnetic features – properties also exploited by nature in ubiquitous iron-sulfur proteins.<sup>8</sup> Of particular relevance are proteins containing chains of Fe<sub>4</sub>S<sub>4</sub> clusters that facilitate electron transport over long distances.<sup>9</sup> Several synthetic examples further demonstrate the utility of Fe<sub>4</sub>S<sub>4</sub> clusters towards building materials with unusual physical and chemical properties. For instance, Kanatzidis and coworkers have prepared a crystalline framework<sup>10</sup> and a family of amorphous chalcogels with Fe<sub>4</sub>S<sub>4</sub> units connected by inorganic chalcogenide linkers. The Fe<sub>4</sub>S<sub>4</sub> clusters retain their redox-activity in the chalcogels, enabling redox catalysis by these materials.<sup>11</sup> Additionally, Pickett and coworkers have studied the synthesis and conductivity of a series of materials in which Fe<sub>4</sub>S<sub>4</sub> clusters are bound to substituted polypyrroles through electrostatic interactions or



**Scheme 1.** Synthesis of [Fe<sub>4</sub>S<sub>4</sub>(BDT)<sub>2</sub>][NR<sub>4</sub>]<sub>2</sub> coordination polymers.

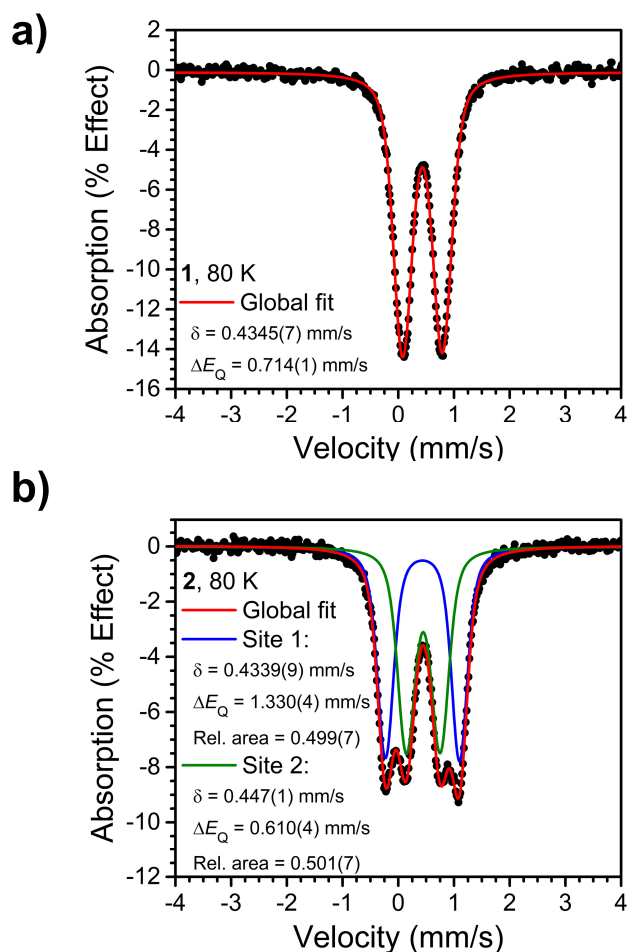


**Figure 1.**  $^{57}\text{Fe}$  Mössbauer spectrum of (a) **1** and (b) **2** recorded at 80 K.

pendant thiolates.<sup>12</sup> These examples illustrate the potential of materials synthesized with  $\text{Fe}_4\text{S}_4$  clusters.

In this work we report the preparation of coordination polymers containing 1D chains of  $\text{Fe}_4\text{S}_4$  clusters linked by an organochalcogenide ligand, 1,4-benzenedithiolate (BDT, Scheme 1). This represents a highly unusual example where  $\text{Fe}_4\text{S}_4$  clusters can be combined with organic linkers to form crystalline coordination polymers. The choice of counterion and solvent controls the packing and solubility of the anionic chains, allowing isolation and characterization of two distinct crystalline solids. The redox-activity of the  $\text{Fe}_4\text{S}_4$  clusters is maintained in the polymer, manifesting as redox-dependent electrical conductivity in the solid materials. These results show the promise of using redox-active metal-chalcogenide clusters as building blocks for coordination polymers with tunable physical properties.

## RESULTS AND DISCUSSION

### Synthesis and Composition

Heating  $[\text{Fe}_4\text{S}_4(\text{SPh})_4][\text{TBA}]_2$  (TBA = tetra-*n*-butylammonium) with 2 equivalents of 1,4-benzenedithiol (BDTH<sub>2</sub>) in *N,N*-dimethylformamide (DMF) leads to the precipitation of  $[(\text{Fe}_4\text{S}_4)(\text{BDT})_2][\text{TBA}]_2$  (**1**) as a dark purple to black solid. Similarly,  $[(\text{Fe}_4\text{S}_4)(\text{BDT})_2][\text{TMA}]_2$  (**2**) is obtained by heating in MeCN when TBA is replaced by tetramethylammonium (TMA) as the counterion. X-ray powder diffraction (XRPD) analysis demonstrates that both of these materials are crystalline. Furthermore, we have observed that the crystallinity of both **1** and **2** can be increased by addition of excess  $[\text{Li}][\text{CF}_3\text{SO}_3]$  to the

reaction mixture. We speculate that this effect may be attributed to ionic screening as discussed below.

We have performed several experiments to validate the proposed compositions of **1** and **2**. Digestion of **1** and **2** in 12 M hydrochloric acid followed by extraction with  $\text{C}_6\text{D}_6$  or  $\text{CD}_2\text{Cl}_2$  and  $^1\text{H}$  NMR analysis supports the presence of BDT in the structures (Figures S4 and S6). No thiophenol from the  $[\text{Fe}_4\text{S}_4(\text{SPh})_4]^{2-}$  starting material is observed, which is also consistent with complete ligand substitution in the precipitated material. The infrared spectra of **1** and **2** do not show any features attributable to S-H stretching modes near  $2500\text{ cm}^{-1}$ , further demonstrating that BDT is fully deprotonated in **1** and **2** (Figures S39 and S40). Additionally, digestion in  $\text{D}_2\text{SO}_4$  followed by dilution with  $(\text{CD}_3)_2\text{SO}$  and  $^1\text{H}$  NMR analysis confirms the presence of TBA in **1** and TMA in **2** (Figures S5 and S7). The presence of intact  $\text{Fe}_4\text{S}_4$  clusters is more difficult to confirm with the same method, as these clusters are not stable to acid digestion. Mössbauer spectroscopy, however, provides strong evidence for the presence of intact  $\text{Fe}_4\text{S}_4$  clusters in **1** and **2**. The 80 K  $^{57}\text{Fe}$  Mössbauer spectrum (Figure 1a) of **1** consists of a quadrupole doublet with isomer shift ( $\delta$ ) of  $0.4345(7)\text{ mm/s}$  and quadrupole splitting ( $\Delta E_Q$ ) of  $0.714(1)\text{ mm/s}$ . These values are similar to those reported for other  $[\text{Fe}_4\text{S}_4]^{2+}$  cluster materials and to  $[\text{Fe}_4\text{S}_4(\text{SPh})_4]^{2-}$ ,<sup>8,10,11b</sup> suggesting that the cluster is present in **1** in the same oxidation state as the  $[\text{Fe}_4\text{S}_4(\text{SPh})_4][\text{TBA}]_2$  precursor. The spectrum (Figure 1b) of **2** can be fitted by two quadrupole doublets with  $\delta$  of  $0.4339(9)$  and  $0.447(1)\text{ mm/s}$  and  $\Delta E_Q$  of  $1.330(4)$  and  $0.610(4)\text{ mm/s}$ , suggesting that two distinct  $[\text{Fe}_4\text{S}_4]$  sites are present in the structure of **2**. All spectra are fit with Voigt line profiles, potentially reflecting a distribution of Mössbauer parameters due to structural disorder.<sup>13</sup> Spectra of **1** and **2** at 25 K and 4.2 K are similar to those at 80 K, showing increases in quadrupole splittings upon cooling (Figures S34, S35).

Additional experiments were performed to verify the empirical formulas of **1** and **2**. X-ray photoelectron spectroscopy (XPS) gives an Fe:S atomic ratio of 1:1.96 and 1:1.95, as expected for **1** and **2** respectively. In addition, inductively-coupled plasma mass spectrometry (ICP-MS) measurements on nitric acid digests of **1** and **2** indicate that little  $\text{Li}^+$  (1.4% and 7% relative to TBA or TMA respectively) is incorporated into the materials (Table S1). Finally, the results from combustion analysis are also consistent for these materials. All of this data supports the assigned formulas of  $[(\text{Fe}_4\text{S}_4)(\text{BDT})_2][\text{TBA}]_2$  and  $[(\text{Fe}_4\text{S}_4)(\text{BDT})_2][\text{TMA}]_2$  for **1** and **2** respectively.

### Structural Determination

The crystal structures of **1** and **2** were solved ab initio using simulated annealing and then further refined with the Rietveld method from synchrotron XRPD data with input from the experimentally determined formulas (Figure 2 and Figure 3). The structure of **1** consists of chains of  $\text{Fe}_4\text{S}_4$  clusters connected by pairs of BDT groups surrounded by TBA cations. Each  $\text{Fe}_4\text{S}_4$  cluster is equidistant from four TBA cations  $5.97\text{ \AA}$  from the  $\text{Fe}_4\text{S}_4$  centroid. The axis-to-axis separation between adjacent chains is  $11.93\text{ \AA}$ , and the separation between  $\text{Fe}_4\text{S}_4$  clusters within the chain is  $9.92\text{ \AA}$  (centroid to centroid). The rings of the BDT linkers in each pair and the Fe atoms to which they are coordinated are coplanar. In the structure of **2**, similar  $\text{Fe}_4\text{S}_4$ -BDT chains are present. In the absence of the bulky TBA cations, the separation between chains decreases to  $8.59\text{ \AA}$  with the TMA cations confined to channels between the chains. Two  $\text{Fe}_4\text{S}_4$  sites alternate along each chain, with distances of  $5.77$  and  $6.77\text{ \AA}$  respectively to each of the nearest four TMA cations. In contrast to **1**, the ring formed by the pair of BDT groups and

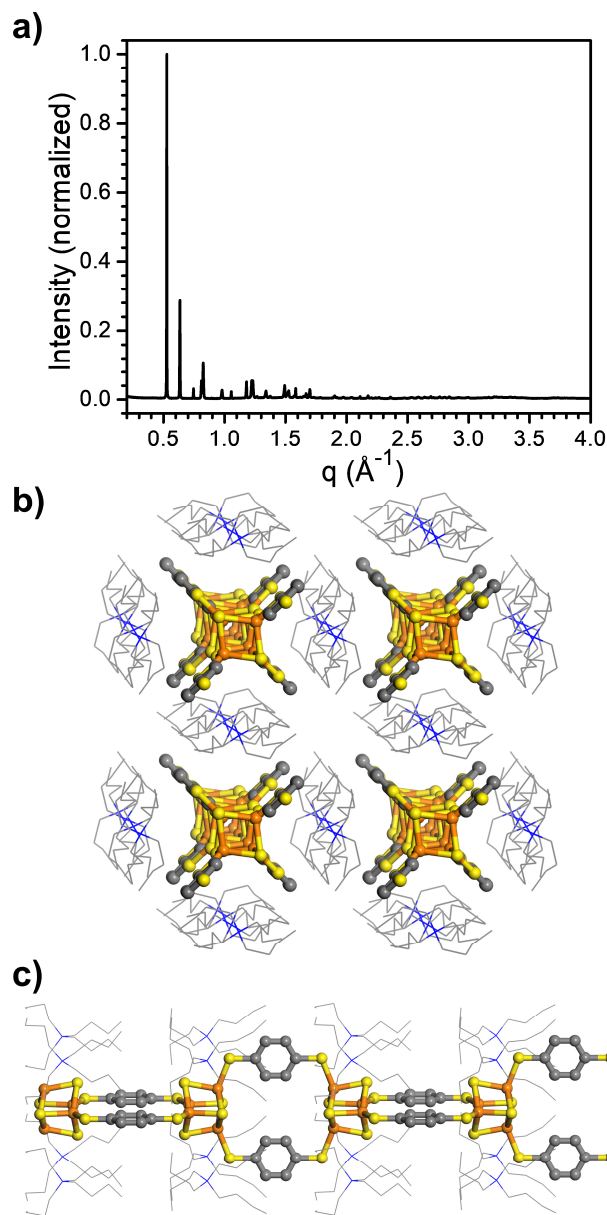


**Figure 2.** X-ray powder diffraction pattern (a) and structure of **1** solved from synchrotron X-ray powder diffraction data viewed (b) parallel to the  $\text{Fe}_4\text{S}_4$ -BDT chain and (c) perpendicular to the chain. Atoms shown as balls and sticks with Fe = orange, S = yellow, C = gray, N = blue; H atoms omitted for clarity; tetrabutylammonium ions are rendered as sticks to highlight the  $\text{Fe}_4\text{S}_4$ -BDT chain.

the  $\text{Fe}_4\text{S}_4$  clusters in **2** is buckled, with a Fe-S-C<sub>6</sub>H<sub>4</sub>-S-Fe dihedral angle of 43.5°. The closest separation between  $\text{Fe}_4\text{S}_4$  clusters is 10.24 Å within each chain and 10.00 Å between chains. The presence of two distinct sites for the  $\text{Fe}_4\text{S}_4$  clusters is consistent with the Mössbauer spectrum of **2**.

We had initially hypothesized that the combination of  $\text{Fe}_4\text{S}_4$  clusters and BDT could produce an extended 3D framework, but the observed 1D structures suggest that other conformations of these materials are accessible. We hypothesize that the choice of cation may be an important point of modulation to control morphology. In **1**, the  $\text{Fe}_4\text{S}_4$ -BDT chains are separated by TBA cations, but in **2**, the smaller TMA cations allow closer contact between the chains. Additionally, the size of the cation is found to affect the conformation of the chains, which

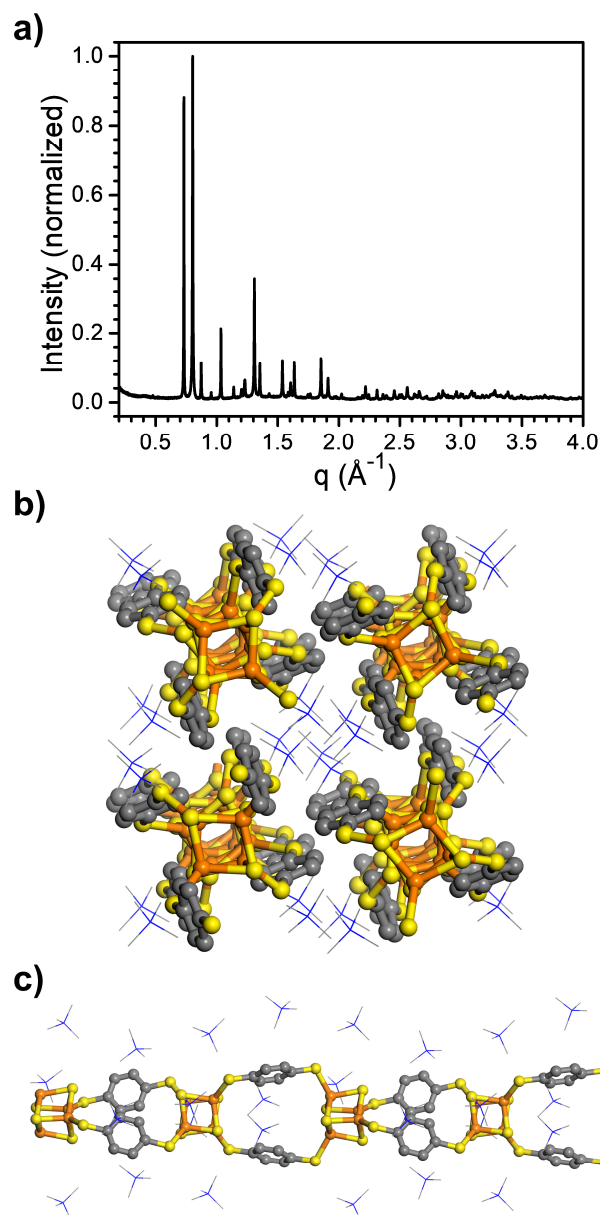


**Figure 3.** X-ray powder diffraction pattern (a) and structure of **2** solved from synchrotron X-ray powder diffraction data viewed (b) parallel to the  $\text{Fe}_4\text{S}_4$ -BDT chain and (c) perpendicular to the chain. Atoms shown as balls and sticks with Fe = orange, S = yellow, C = gray, N = blue; H atoms omitted for clarity; tetramethylammonium ions are rendered as sticks to highlight the  $\text{Fe}_4\text{S}_4$ -BDT chain.

highlights that the coordination of BDT to Fe is flexible. The different structures imbued by these cations, as well as the different synthetic conditions required to isolate **2**, prompted us to investigate the solution phase behavior of these materials.

#### Solution Behavior of $\text{Fe}_4\text{S}_4$ -BDT Chains

The observation that addition of  $\text{Li}^+$  during synthesis of **1** and **2** slows the rate of precipitation and improves crystallinity led us to hypothesize that the  $\text{Fe}_4\text{S}_4$ -BDT chains might form in solution prior to packing with TBA or TMA and subsequent precipitation. We note that initial attempts to synthesize **2** by heating of BDTH<sub>2</sub> with  $[\text{Fe}_4\text{S}_4(\text{SPh})_4][\text{TMA}]_2$  in DMF resulted in negligible formation of a precipitate (in some cases, a small amount of an amorphous solid degradation product formed and was

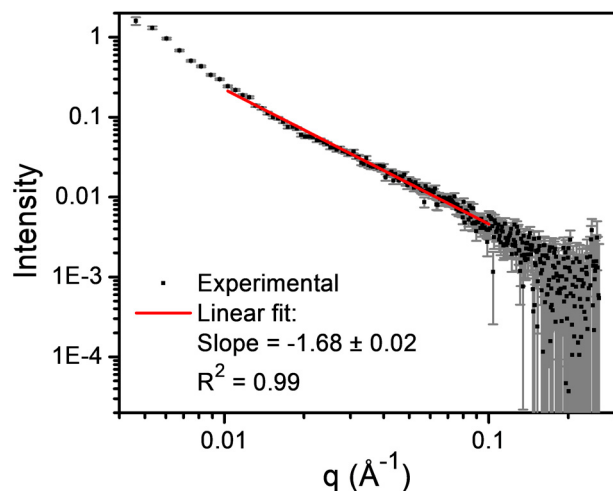


**Figure 4.** Small angle X-ray scattering (SAXS) from a DMF solution of **2**.

filtered out). Furthermore, addition of 5 equivalents of [TBA][PF<sub>6</sub>] to this solution after cooling to room temperature resulted in rapid precipitation of poorly-crystalline **1**. This suggests that chains of **2** may be forming in solution but are sufficiently soluble in DMF to avoid precipitation. Addition of [TBA][PF<sub>6</sub>] then putatively triggers rapid packing of the chains which forces the observed precipitation.

To test this hypothesis the solubility of isolated **2** was also investigated. Isolated crystalline **2** is soluble in DMF, and addition of [TBA][PF<sub>6</sub>] to this solution also results in the immediate precipitation of poorly-crystalline **1**. This precipitation can be slowed by the addition of excess [Li][CF<sub>3</sub>SO<sub>3</sub>], suggesting that ionic strength likely plays a role in ion packing and hence in controlling the rate of crystallization (Figure S47). In this way, the [Li][CF<sub>3</sub>SO<sub>3</sub>] may act similarly to the competing ligands often used as modulators in syntheses of MOFs.<sup>14</sup> The use of non-coordinating salts as modulators is less explored, but ionic strength has been invoked as a factor affecting the dynamics of other soluble coordination polymers.<sup>15</sup> To further examine the solution structure of these chains, small angle X-ray scattering (SAXS) experiments were carried out on a near-saturated DMF solution of **2** (Figure 4). The SAXS data are best fit to a power-law behavior at higher  $q$ , with a slope on a log-log plot near  $-5/3$  that is indicative of a swollen polymer coil structure.<sup>16</sup> The full range of data can also be fit well by the unified exponential/power-law model described by Beaucage,<sup>16</sup> yielding a similar result (Figure S23). This type of scattering has been reported for other charged polymers such as DNA.<sup>17</sup> Taken together, these results indicate that the Fe<sub>4</sub>S<sub>4</sub>-BDT chain persists in solution, and it seems that the identity of the counterion plays an important role in solubility and crystallization.

The Fe<sub>4</sub>S<sub>4</sub>-BDT chains found in both **1** and **2** contain Fe<sub>4</sub>S<sub>4</sub> clusters with a similar separation to those in biological electron transport chains.<sup>9,18</sup> This raises the possibility that electrical conductivity could occur along these chains. Furthermore, we hypothesized that the shorter chain-chain contacts in **2** might also facilitate enhanced electronic coupling. As such, we next investigated the electronic structure and conductivity of these materials.

#### Electronic Properties of Fe<sub>4</sub>S<sub>4</sub>-BDT Chains

The diffuse reflectance UV-visible spectra of **1** and **2** (Figure 5) show a broad band near 560 nm, along with a shoulder near 820 nm and additional absorption in the UV region. Solutions

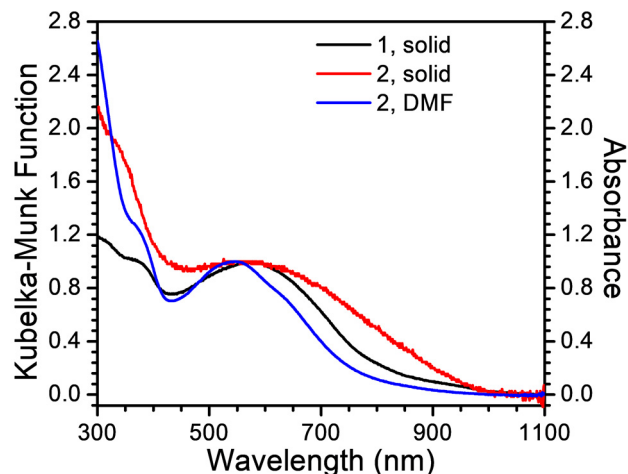


**Figure 5.** Normalized UV-visible diffuse reflectance spectra of **1** and **2** in a [Mg][SO<sub>4</sub>] matrix plotted as a Kubelka-Munk function and absorbance spectrum of **2** in DMF solution.

of **2** in DMF show similar features, providing further evidence that the Fe<sub>4</sub>S<sub>4</sub>-BDT chains persist in solution. The 560 nm feature is red-shifted from the 450 nm absorption observed for monomeric [Fe<sub>4</sub>S<sub>4</sub>(SPh)<sub>4</sub>]<sup>2-</sup> in solution (Figure S26). This band has been attributed to a ligand-to-metal charge transfer transition involving the thiolate ligand.<sup>19</sup> The more electron rich nature of the BDT ligand in **1** versus the thiophenolate ligand in the monomer may explain this shift.

The electron transfer series of biologically relevant cubane-type Fe<sub>4</sub>S<sub>4</sub> clusters has been studied extensively. Of these, the [Fe<sub>4</sub>S<sub>4</sub>]<sup>2+</sup> and [Fe<sub>4</sub>S<sub>4</sub>]<sup>+</sup> cores are the most stable and thoroughly characterized oxidation states.<sup>20</sup> The redox behavior of these Fe<sub>4</sub>S<sub>4</sub>-BDT chains was investigated by cyclic voltammetry (CV) on DMF solutions of **2** (Figure 6). These measurements are complicated by the dependence of solubility on counterion as noted above. When 0.1 M [TMA][PF<sub>6</sub>] is used as the electrolyte, the Fe<sub>4</sub>S<sub>4</sub>-BDT chains partially precipitate as an amorphous solid, forming a fine suspension. We suspect that this precipitation is due to a much higher concentration of TMA as compared with the conditions for the synthesis of **2**. When 0.1 M [Li][CF<sub>3</sub>SO<sub>3</sub>] is used instead, no precipitation is observed. With [TMA][PF<sub>6</sub>] as the electrolyte, the CV response of this

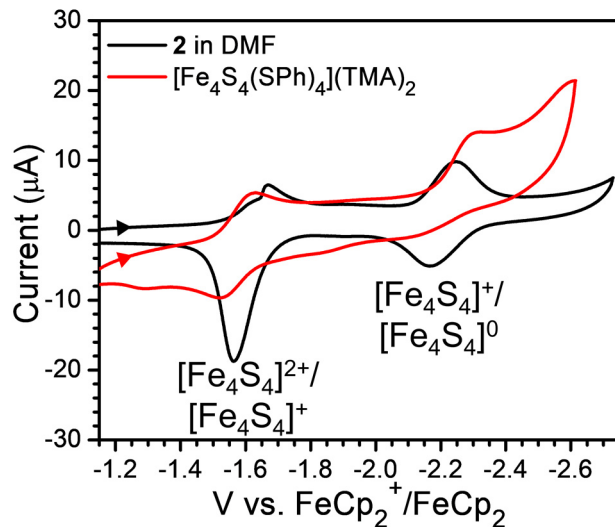


**Figure 6.** Cyclic voltammograms of **2** and monomeric [Fe<sub>4</sub>S<sub>4</sub>(SPh)<sub>4</sub>][TMA]<sub>2</sub>. Arrow denotes scan direction. Conditions: DMF, 0.1 M [Li][CF<sub>3</sub>SO<sub>3</sub>], 0.1 V/s.

suspension is similar to that of the  $[\text{Fe}_4\text{S}_4(\text{SPh})_4][\text{TMA}]_2$  monomer in solution (Figure S43), showing quasi-reversible reductions at  $-1.43$  and  $-2.13$  V vs.  $\text{FeCp}_2^+/\text{FeCp}_2$  (Figure S44). With  $[\text{Li}][\text{CF}_3\text{SO}_3]$  as the electrolyte, reductive features are similarly observed at  $-1.6$  and  $-2.2$  V vs.  $\text{FeCp}_2^+/\text{FeCp}_2$  (Figure 6). By comparison to the monomer, these features correspond to the  $[\text{Fe}_4\text{S}_4]^{2+}/[\text{Fe}_4\text{S}_4]^+$  and  $[\text{Fe}_4\text{S}_4]^+/\text{Fe}_4\text{S}_4^0$  redox couples. Upon scanning past the first reductive feature in  $[\text{Li}][\text{CF}_3\text{SO}_3]$  electrolyte, a deposit is observed on the working electrode which redissolves at more oxidizing potentials. This suggests that the  $\text{Fe}_4\text{S}_4$ -BDT chain containing  $[\text{Fe}_4\text{S}_4]^+$  clusters is less soluble, and may explain the non-ideal shape of the CV features and changes upon repeated scans (Figure S46). Despite this complexity, the electrochemistry results demonstrate that the redox-activity of the  $\text{Fe}_4\text{S}_4$  clusters is preserved in the  $\text{Fe}_4\text{S}_4$ -BDT chains present in **2** and likely in **1** as well.

In addition to these reductive features, an irreversible oxidation was observed at approximately  $-0.3$  V vs.  $\text{FeCp}_2^+/\text{FeCp}_2$  with both electrolytes. Because bulky ligands have been shown to improve the stability of the  $[\text{Fe}_4\text{S}_4]^{3+}$  oxidation state,<sup>21</sup> we had hypothesized that this state might be stabilized in a coordination polymer. However, the irreversible oxidation near the potential observed in the monomer suggests that this is not the case for the  $\text{Fe}_4\text{S}_4$ -BDT chains in solution or suspension.

As-synthesized **1** and **2** are both poor electrical conductors, with room temperature pressed pellet conductivities of  $\sigma = 3(3) \times 10^{-11}$  S/cm and  $5(3) \times 10^{-10}$  S/cm respectively. For comparison, the conductivities of the monomeric starting materials ( $[\text{Fe}_4\text{S}_4(\text{SPh})_4][\text{TBA}]_2$  and  $[\text{Fe}_4\text{S}_4(\text{SPh})_4][\text{TMA}]_2$ ) are both below  $10^{-12}$  S/cm. The similarity in values for **1** and **2** suggests that insulation of the  $\text{Fe}_4\text{S}_4$ -BDT chains by the large TBA cation is not the only factor leading to low conductivity. Instead, we propose that these insulating behaviors may be ascribed to two factors. Firstly, there is likely a low concentration of charge carriers along the chain due to the  $S = 0$  ground state of  $[\text{Fe}_4\text{S}_4]^{2+}$ . Secondly, we note the observed bulk conductivity of pressed pellet samples is a weighted average of the conductivity in each crystallographic direction plus grain boundary resistance. Both of these factors will lower the measured conductivity.<sup>22</sup>

Doping experiments were carried out to introduce additional charge carriers and improve the conductivities of these materials. Solid **1** and **2** were soaked in a THF solution containing 0.5 equivalents of bis(pentamethylcyclopentadienyl)cobalt(II) ( $\text{CoCp}^*_2$ ) per  $\text{Fe}_4\text{S}_4$  unit and excess  $[\text{Li}][\text{CF}_3\text{SO}_3]$ . The reductively-doped analogues of **1** and **2** exhibited enhanced conductivities of  $6(2) \times 10^{-9}$  S/cm and  $5(2) \times 10^{-6}$  S/cm respectively. In contrast, similar doping experiments with an oxidizing agent, ferrocenium tetrafluoroborate ( $[\text{Fc}][\text{BF}_4]$ ), in the presence of excess  $[\text{TMA}][\text{Br}]$  resulted in no measurable

enhancement ( $7(5) \times 10^{-12}$  S/cm and  $7(1) \times 10^{-10}$  S/cm for **1** and **2** respectively). The crystallinity of all doped materials was maintained as verified by their XRPD patterns (Figures S15-S18).

Reduction of the  $[\text{Fe}_4\text{S}_4]^{2+}$  cluster requires incorporation of an additional cation for charge balance, either  $\text{Li}^+$  or  $\text{CoCp}^*_2$ . ICP-MS was therefore used to assess the degree of reduction in **1** and **2** (Table 1). For analysis of the ICP-MS data, it is assumed that exchange of TBA or TMA with  $\text{Li}^+$  or  $\text{CoCp}^*_2$  does not occur. This assertion is supported by the observation that the  $\text{Li}^+$  content in **1** and **2** does not increase upon soaking in a THF solution of  $[\text{Li}][\text{CF}_3\text{SO}_3]$  without reductant. The increase in Li and Co content upon treatment indicates reduction by 0.07(2) and 0.24(6) electrons per formula unit for **1** and **2** respectively. The lower degree of reduction in **1** is consistent with the smaller increase in conductivity upon treatment and may be due to difficulty incorporating the additional cations into the densely packed structure. Mössbauer spectroscopy was used to further characterize the reduced materials (Figures S33-S37). For both **1** and **2**, the spectra of the reduced materials show no additional signals attributable to free  $\text{Fe}^{2+}$  or  $\text{Fe}^{3+}$ ,<sup>23</sup> indicating that the  $\text{Fe}_4\text{S}_4$  clusters remain intact. Mössbauer spectra of monomeric  $\text{Fe}_4\text{S}_4$  clusters show small increases in isomer shift and quadrupole splitting upon reduction from  $[\text{Fe}_4\text{S}_4]^{2+}$  to  $[\text{Fe}_4\text{S}_4]^+$ .<sup>23,24</sup> With **1**, no significant changes are seen in the Mössbauer spectra, consistent with the small degree of reduction estimated from ICP-MS. In contrast, the spectrum of **2** shows small changes in shape (Figure S37). This suggests an additional, unresolved contribution from a species with higher isomer shift than the as-synthesized **2**. Subtraction of the spectra of the as-synthesized and reduced materials reveals a broad additional signal in the same region as literature spectra of  $[\text{Fe}_4\text{S}_4]^+$  compounds (Figure S38).<sup>23</sup> This contribution can be approximated in fits to the spectrum of reduced **2** by addition of a third site with similar  $\delta$  and  $\Delta E_Q$  to literature  $[\text{Fe}_4\text{S}_4]^+$  spectra (full treatment of the  $[\text{Fe}_4\text{S}_4]^+$  species with two Fe sites was not possible given the low intensity of this feature and overlap with signals from  $[\text{Fe}_4\text{S}_4]^{2+}$  sites). These changes are reversible by brief exposure to dry air, further supporting their attribution to reduced  $[\text{Fe}_4\text{S}_4]^+$  clusters. While interpretation of the Mössbauer spectra is complicated by the presence of overlapping signals, these data support that the reversible redox-activity of the  $\text{Fe}_4\text{S}_4$  clusters is preserved.

Finally, we have also investigated chemical reduction of **2** in the solution phase. Upon treatment with approximately 0.5 equivalents of sodium acenaphthylene ( $[\text{Na}][\text{C}_{12}\text{H}_8]$ ), DMF solutions of **2** show changes in their UV-visible absorption spectra consistent with partial reduction of the  $\text{Fe}_4\text{S}_4$  clusters from  $[\text{Fe}_4\text{S}_4]^{2+}$  to  $[\text{Fe}_4\text{S}_4]^+$  (Figure S27).<sup>25</sup> A small amount of precipitate was observed, consistent with the lower solubility of the reduced polymer observed during cyclic voltammetry experiments. SAXS and IR measurements support the persistence of the polymer structure in the reduced solution (Figures S24, S25, S41, S42). Following precipitation of the partially reduced solution by addition of  $\text{Et}_2\text{O}$ , an amorphous solid was obtained with conductivity of  $1.5(5) \times 10^{-5}$  S/cm. In contrast, material precipitated from a DMF solution of **2** without added reductant showed a conductivity of  $3(4) \times 10^{-9}$  S/cm. ICP-MS measurements of the Na/Fe ratio were used to assess the degree of reduction between these two materials. These data indicate that the material was reduced by 0.6(4) electrons per cluster. This result further supports that the introduction of charge carriers by accessing the  $[\text{Fe}_4\text{S}_4]^+$  oxidation state is advantageous for preparing materials with enhanced electrical conductivity.

**Table 1.** Li and Co content of **1** and **2** before and after reduction in the solid state

Molar ratio	Compound Reduced <b>1</b>	Compound Reduced <b>2</b>
Li/ $\text{Fe}_4\text{S}_4$		
Before reduction	3(1)%	14(5)%
After reduction	9(1)%	28(4)%
Increase amount	6(2)%	15(6)%
Co/ $\text{Fe}_4\text{S}_4$		
Before reduction	0.14(4)%	0.08(2)%
After reduction	1.2(3)%	9.0(6)%
Increase amount	1.1(3)%	9.0(6)%
Reduction degree	7(2)%	24(6)%

## CONCLUSION

We have synthesized and characterized two new materials incorporating redox-active Fe<sub>4</sub>S<sub>4</sub> clusters with an organochalcogenide ligand, BDT. Synchrotron X-ray powder diffraction data analysis revealed that the materials feature 1D chains of Fe<sub>4</sub>S<sub>4</sub> clusters connected by pairs of BDT ligands. Small angle X-ray scattering measurements and precipitation experiments proved the persistence of these chains in solution. The choice of counterion is important in determining the packing and solubility of these anionic chains. Mössbauer spectroscopy and cyclic voltammetry demonstrate that the redox-activity of the Fe<sub>4</sub>S<sub>4</sub> cluster is preserved in these materials, and chemical reduction is shown to impart enhanced electrical conductivity. These results lay the groundwork for a new class of materials based on metal-sulfur clusters with organosulfur ligands.

## EXPERIMENTAL

### General Methods

All manipulations were performed under an inert atmosphere of dry N<sub>2</sub> using a Schlenk line or MBraun UNIlab glovebox unless otherwise noted. <sup>1</sup>H NMR measurements were performed on Bruker DRX 400 or 500 spectrometers. Elemental analyses (C, H, N) were performed by Midwest Microlabs. Inductively coupled plasma mass spectrometry (ICP-MS) data was obtained with an Agilent 7700x ICP-MS and analyzed using ICP-MS Mass Hunter version B01.03. The samples were diluted in 2% HNO<sub>3</sub> matrix and analyzed with a <sup>159</sup>Tb internal standard against a 12-point standard curve over the range from 0.1 ppb to 500 ppb. The correlation was > 0.9997 for all analyses of interest. Data collection was performed in Spectrum Mode with five replicates per sample and 100 sweeps per replicate. Dimethylformamide (DMF), tetrahydrofuran (THF), and acetonitrile (MeCN) used in preparing the coordination polymers were initially dried and purged with Ar on a solvent purification system from Pure Process Technology. DMF was then passed through activated alumina before use. THF was stirred with liquid NaK alloy and then filtered through activated alumina and stored over 4 Å molecular sieves. MeCN was stored over 4 Å molecular sieves. Dimethylacetamide (DMA) was sparged with N<sub>2</sub>, transferred into the glovebox, passed through activated alumina and stored over 4 Å molecular sieves. [TMA][PF<sub>6</sub>] was recrystallized from H<sub>2</sub>O and dried at 160 °C before use.<sup>26</sup> All other chemicals were purchased from commercial sources and used as received. [Fe<sub>4</sub>S<sub>4</sub>(SPh)<sub>4</sub>][TBA]<sub>2</sub> was prepared as previously described.<sup>27</sup>

### Synthetic Procedures

#### 1,4-Bis(isopropylthio)benzene

1,4-Bis(isopropylthio)benzene was synthesized following a reported procedure,<sup>28</sup> but the synthetic method and purification have been modified as follows:

A dispersion of 60% NaH in mineral oil (19.2 g, 480 mmol) was added to a 500 mL three-neck flask and then washed with hexane twice and DMA once under a N<sub>2</sub> atmosphere. After adding DMA (100 mL), 2-propanethiol (52 mL, 480 mmol) was injected slowly and in portions to avoid excessive foaming (if necessary, use of ice bath and drop funnel is helpful). Subsequently, DMA (100 mL) and a solution of 1,4-dibromobenzene (28.3 g, 120 mmol) in DMA (150 mL) were injected, and the mixture was heated for 17 h to 100 °C. The mixture was cooled, poured into 100 mL saturated NaCl solution and extracted with Et<sub>2</sub>O (3×100 mL). The organic layer was washed with H<sub>2</sub>O (5×50 mL), dried with [Mg][SO<sub>4</sub>], and evaporated. The yellowish oil was further purified by vacuum distillation. Yield: 22 g

(82%). Ref. b.p. 168-169 °C. <sup>1</sup>H NMR (400 MHz, CDCl<sub>3</sub>): δ 7.31 (4 H, s), 3.36 (2 H, spt, J = 3.4 Hz), 1.28 (12 H, d, J = 1.3 Hz) ppm.

#### 1,4-Benzenedithiol

*Safety note: In our experience any excess Na was consumed by side reactions with the solvent and was not present after heating. However, care should be taken to ensure that no Na metal is present before adding the HCl solution. Addition of a few drops of the acid solution first is recommended to check for bubbling that would indicate the presence of Na metal.*

Sodium (1.8 g, 80 mmol), dry DMA (40 mL) from the glovebox, and 1,4-Bis(isopropylthio)benzene (4.5 g, 20 mmol) were added in sequence to a 125 mL three-neck flask under N<sub>2</sub> atmosphere and the mixture was heated to 100 °C for 8 h. During this time the reaction mixture became thick with precipitate. The reaction solution was quenched with diluted HCl solution (concentrated HCl solution (34-37% w/w, 10 mL) + H<sub>2</sub>O (50 mL)) in an ice bath and stirred for another 0.5 h under an inert atmosphere. The mixture was extracted with Et<sub>2</sub>O (2×75 mL). The organic layer was washed with H<sub>2</sub>O (5×30 mL), dried with [Mg][SO<sub>4</sub>], and evaporated. A white powder was obtained by washing with hexanes (20 mL). More product can be recovered by storing the hexane washes in a freezer (-35 °C) overnight, resulting in a pale yellow to white powder. Overall yield: 1.9 g (67%). <sup>1</sup>H NMR (400 MHz, CDCl<sub>3</sub>): δ 7.16 (4 H, s) and 3.41 (2 H, s) ppm.

#### [Fe<sub>4</sub>S<sub>4</sub>(SPh)<sub>4</sub>][TMA]<sub>2</sub>

*The synthesis of this compound has been reported previously,<sup>29</sup> but details of the synthetic method and purification had not been published.*

MeOH (80 mL) was added to a 250 mL Schlenk flask with a stir bar and deoxygenated by four pump-purge cycles with N<sub>2</sub>. The flask was then cooled in an ice/water bath. Sodium (1.8 g, 80 mmol) was added with stirring and continued cooling and allowed to dissolve fully before returning the flask to room temperature. PhSH (8.2 mL, 80 mmol) was then injected into the reaction mixture. In a separate 250 mL Schlenk flask, anhydrous FeCl<sub>3</sub> (3.2 g, 20 mmol) and MeOH (50 mL) were deoxygenated by four pump-purge cycles with N<sub>2</sub> and transferred via cannula to the flask containing the [Na][PhS] solution. Sulfur (0.64 g, 20 mmol) was added and the reaction mixture stirred overnight at room temperature. This mixture was then filtered into a solution of [TMA][Br] (2.3 g, 15 mmol) in methanol (45 mL), resulting in precipitation of the crude product as a black solid. This suspension was filtered and the resulting solid dried under vacuum. The crude solid was dissolved in ~70 °C deoxygenated MeCN (40 mL) and passed through a glass frit before deoxygenated MeOH (130 mL) was added via slow cannula transfer while heating to ~60 °C. Slow cooling of this solution to -35 °C resulted in the formation of large black crystals that were collected by filtration, washed with MeOH, and dried under vacuum (4.0 g, 85%). <sup>1</sup>H NMR (400 MHz, CD<sub>3</sub>CN): δ 8.19 (8 H, d, J = 5.7 Hz), 5.91 (8 H, br. s), 5.30 (4 H, t, J = 5.6 Hz), 3.07 (24 H, s) ppm.

#### [Fe<sub>4</sub>S<sub>4</sub>(BDT)<sub>2</sub>][TBA]<sub>2</sub> (**1**)

[Fe<sub>4</sub>S<sub>4</sub>(SPh)<sub>4</sub>][TBA]<sub>2</sub> (192 mg, 0.15 mmol) and [Li][CF<sub>3</sub>SO<sub>3</sub>] (117 mg, 0.75 mmol) were added to a 24 mL vial and dissolved in DMF (12 mL). A solution of 1,4-benzenedithiol (43 mg, 0.30 mmol) in DMF (3 mL) was added and the vial was sealed and placed in a heating block on a 140 °C hot plate. The reaction mixture was heated for 2 days, after which **1** was separated by centrifugation, washed with DMF (4×2 mL) and THF (3×2 mL), and dried under vacuum. Compound **1** was obtained as a black

powder (102 mg, 61%). Anal. calc. for  $\text{Fe}_4\text{S}_8\text{C}_{44}\text{H}_{80}\text{N}_2$ : C 47.31%, H 7.22%, N 2.51%; found: C 44.61%, H 6.62%, N 2.18%. The combustion analysis for this material is improved upon soaking with excess TBA (see below).

#### [ $\text{Fe}_4\text{S}_4(\text{BDT})_2$ ][ $\text{TMA}$ ]<sub>2</sub> (**2**)

[ $\text{Fe}_4\text{S}_4(\text{SPh})_4$ ][ $\text{TMA}$ ]<sub>2</sub> (140 mg, 0.15 mmol) and [ $\text{Li}$ ][ $\text{CF}_3\text{SO}_3$ ] (936 mg, 6.0 mmol) were added to a 24 mL vial and dissolved in MeCN (9 mL). A solution of 1,4-benzenedithiol (43 mg, 0.30 mmol) in MeCN (6 mL) was added and the vial was sealed and placed in a heating block on a 100 °C hot plate. The reaction mixture was heated for 2 days, after which **2** was separated by centrifugation, washed with MeCN (4x2 mL), and dried under vacuum. **2** was obtained as a black powder (68 mg, 58%). Anal. calc. for  $\text{Fe}_4\text{S}_8\text{C}_{20}\text{H}_{32}\text{N}_2$ : C 30.78%, H 4.13%, N 3.59%; found: C 30.46%, H 4.11%, N 3.62%.

#### Reductive doping experiments of solid state **1** and **2**

**1** (0.05 mmol, 56 mg) or **2** (0.05 mmol, 39 mg) was soaked in a solution of  $\text{CoCp}^*_2$  (0.5 equivalents, 0.025 mmol, 8 mg) and excess [ $\text{Li}$ ][ $\text{CF}_3\text{SO}_3$ ] (5 equivalents, 0.25 mmol, 39 mg) in THF (5 mL) and then stirred at room temperature overnight. The reduced product was isolated by centrifugation, washed with THF (typically 4x2 mL) until the wash solvent was colorless, and dried under vacuum. Crystallinity was maintained as verified by XRPD (Figures S15 and S17). The degree of reduction was analyzed by ICP-MS (Table S2).

#### Oxidative doping experiments of solid state **1** and **2**

**1** (0.05 mmol, 56 mg) or **2** (0.05 mmol, 39 mg) was soaked in a solution of [ $\text{Fc}$ ][ $\text{BF}_4$ ] (0.5 equivalents, 0.025 mmol, 7 mg) and excess [ $\text{TMA}$ ][ $\text{Br}$ ] (5 equivalents, 0.25 mmol, 38 mg) in MeCN (4 mL) and MeOH (1 mL) and then stirred at room temperature overnight. The oxidized product was isolated by centrifugation, washed with MeCN (typically 4x2 mL) until the wash solvent was colorless, and dried under vacuum. Crystallinity was maintained as verified by XRPD (Figures S16 and S18).

#### Chemical reduction of **2** in solution

The concentration of **2** in DMF was determined by inductively-coupled plasma optical emission spectroscopy (ICP-OES). Three aliquots of each solution batch were dried, digested in  $\text{HNO}_3$ , and the Fe content was measured versus a Cu internal standard.

A solution of [ $\text{Na}$ ][ $\text{C}_{12}\text{H}_8$ ] was prepared in THF (2.5 mL) by stirring sodium (10 mg, 0.43 mmol) and excess acenaphthylene (80 mg, 0.53 mmol) at room temperature overnight. This solution was passed through a glass microfiber filter and diluted 10-fold with DMF prior to use.

The [ $\text{Na}$ ][ $\text{C}_{12}\text{H}_8$ ] solution (0.5 equivalents, 1.24 mL, 0.022 mmol) was added dropwise to a stirred solution of **2** in DMF (27 mL, 34 mg, 0.043 mmol) and then stirred overnight. The reduced solid was precipitated by addition of an equal volume  $\text{Et}_2\text{O}$  and then separated by centrifugation, washed with THF (4x2 mL), and dried under vacuum. The material was amorphous as checked by XRPD.

#### Treatment with [ $\text{R}_4\text{N}$ ][ $\text{PF}_6$ ]

A mixture of **1** or **2** (0.05 mmol, 55 mg or 39 mg) and a solution of [ $\text{TBA}$ ][ $\text{PF}_6$ ] or [ $\text{TMA}$ ][ $\text{PF}_6$ ] respectively (0.25 mmol, 67 mg or 55 mg) in DMF/MeCN (5 mL) was stirred overnight at 100 °C in the glovebox. In the next morning, the solid was isolated by centrifugation and washed with fresh DMF/MeCN (3x2 mL) and THF (3x2 mL). After drying for hours under vacuum, the crystallinity was still maintained, as examined by

XRPD (Figures S13 and S14). Further ICP-MS analysis suggested that the Li content decreases (Table S1). The C, H, N analysis results of as-synthesized **1** with [ $\text{Li}$ ][ $\text{CF}_3\text{SO}_3$ ] deviate from the theoretical values slightly but by washing with [ $\text{TBA}$ ][ $\text{PF}_6$ ], the C, H, N analysis matches with the assigned formula. Anal. calc. for **1**,  $\text{Fe}_4\text{S}_8\text{C}_{44}\text{H}_{80}\text{N}_2$ : C 47.31%, H 7.22%, N 2.51%; found: C 47.40%, H 7.33%, N 2.36%.

#### Digestion Experiments

**1** and **2** (~5 mg) were digested in 12 M hydrochloric acid (~1 mL) under air to check for BDT and PhSH content. The acid solution was extracted with  $\text{C}_6\text{D}_6$  or  $\text{CD}_2\text{Cl}_2$  (~0.5-1 mL; in the presence of TBA, Fe-containing digestion products were found to be soluble in  $\text{CD}_2\text{Cl}_2$ ) and analyzed by  $^1\text{H}$  NMR spectroscopy.

To test for the presence of quaternary ammonium ions, **1** and **2** (~5 mg) were digested in  $\text{D}_2\text{SO}_4$  (~0.1-0.2 mL),<sup>30</sup> resulting in oxidation of BDT to an insoluble polymer. This suspension was diluted with  $(\text{CD}_3)_2\text{SO}$  and analyzed by  $^1\text{H}$  NMR spectroscopy. Addition of [ $\text{TBA}$ ][ $\text{PF}_6$ ] or [ $\text{TMA}$ ][ $\text{Cl}$ ] standards was used to confirm the identity of the species in solution.

#### Sample Preparation for ICP-MS

Solutions for ICP-MS were prepared by digesting 2 mg of material in 2 mL  $\text{HNO}_3$  (trace metal grade) solution in a fume hood overnight at room temperature. Samples analyzed for Na content were digested in polypropylene to avoid contamination of Na from glass containers. The solution was diluted with ultra-filtered deionized water for ICP-MS analysis. Reported errors are the standard deviation of measurements on three batches of each material, except for the Co content before reduction (measured in duplicate).

#### X-ray Powder Diffraction

##### Reaction screening:

X-ray powder diffraction measurements for screening reaction conditions were performed on a SAXSLAB Ganesha equipped with a Xenocs GeniX3D Cu  $\text{K}\alpha$  source. Samples were loaded into 0.8-1.1 mm ID, 0.25 mm wall borosilicate capillaries and sealed with wax under  $\text{N}_2$ . Data reduction/integration was performed using Saxsui software and a background correction for the capillary was applied.

11-BM APS synchrotron beamline (bending magnet source) / Argonne National Laboratory (Lemont, IL, USA):

The samples were loaded into 1.0 mm OD, 0.01 mm wall borosilicate capillaries in a  $\text{N}_2$ -filled glovebox (using an ionizer to reduce static and repeatedly dropping the capillary into a glass vial) and then capped with a septum with a small amount of vacuum grease. Capillaries were then evacuated via an inserted needle through a septum, and sealed using an electric arc lighter. The powders were rotated during the measurement at ~50 cycles per second. The powder patterns were measured at 295 K at beamline 11-BM of the Advanced Photon Source at Argonne National Laboratory using a wavelength of  $\lambda = 0.41275$  Å, from 0.5 to 50° 2 $\theta$  with a step size of 0.001° and a counting time of 0.1 sec/step.

PROXIMA 2A / SOLEIL synchrotron beamline (Saint-Aubin, France):

To confirm the stability of **1** under the intense X-ray beam of the synchrotron (~1 hour under the beam at APS at ambient conditions), additional powder X-ray diffraction data for **1** were recorded at the PROXIMA 2A beamline (PX2A) of the SOLEIL synchrotron (E = 17 keV,  $\lambda = 0.7293$  Å) using an EIGER X9M 2D hybrid photon counting detector and measured at 295

K.<sup>31</sup> The optical layout included a cryogenically cooled channel-cut Si [111] monochromator, a convex horizontal prefocusing mirror and a pair of focusing bimorph mirrors in Kirpatrick-Baez configuration, resulting in a 100  $\mu\text{m}$  wide X-ray beam at the sample position. The 2D detector was set at a distance of 300 mm from the sample. **1** was packed in a flame-sealed 1.0 mm diameter glass capillary, which was not only rotated during the measurement, but was also translated along its spinning axis, resulting in a helical path of the beam along the exterior of the capillary, all to minimize sample damage from the intense X-ray beam. The capillary was translated along a 0.8 mm path (i.e. ca. 10 times the horizontal beamsize). The measurement time was 72 s, much smaller than for the 11-BM/APS related measurement, making radiation damage to the sample very unlikely. The 2D nature of the measurement, a 2D image displaying full Debye-Scherrer rings, provided a direct check for the maintenance of the crystallinity and homogeneity of the sample, as well as for the absence of significant preferred orientation in the latter (Figure S8).

The free ALBULA / DECTRIS software was used to convert the PX2A synchrotron data from 2D I(x,y) binary frames (CBF & HDF5 formats) into conventional 1D ASCII I(2 $\theta$ ) XRPD histograms, with an average 2 $\theta$  step size of 0.015 $^\circ$ .<sup>32</sup> For both the 11-BM/APS and the PX2A/SOLEIL data, the two ubiquitous indexing programs DICVOL14<sup>33</sup> and N-TREOR14<sup>34</sup> were used, together with their respective graphical interfaces PreDICT<sup>35</sup> and EXPO2014,<sup>36</sup> yielding nearly identical unit cells for a given 1D histogram (Tables S2, S3). For structure solution, the 11-BM data for **1** and **2** were used and simulated annealing applied as implemented in EXPO2014<sup>36</sup> and FOX,<sup>37</sup> yielding similar starting models albeit with different success rates. The Rietveld least-squares refinement of the structure solutions against the synchrotron data was carried out using the GSAS-I software,<sup>38</sup> based on starting models obtained with FOX. Restraints for bond distances and bond angles were introduced in the refinements based on published Fe<sub>4</sub>S<sub>4</sub> cubane structures,<sup>39</sup> as well as from geometry information gathered from the CCDC/MOGUL module of the Cambridge Structural Database (CSD).<sup>40</sup> Besides appraisal of the usual figures of merit for powder structures, the crystallographic arrangements were also analyzed graphically using the CCDC Mercury software<sup>41</sup> to ensure that the obtained refined crystallographic structures were chemically plausible. It is worth noting that even the PX2A data allowed for a successful structure solution, and not merely for successful indexing and Rietveld refinement. Eventually, the two GSAS-I Rietveld-refined structures for both **1** and **2** were obtained as CIF (Crystallographic Information; CCDC 1869639-1869640) files which were themselves validated by the standard IUCr / CheckCIF procedure.<sup>42</sup> Details of the structure solution and refinement are listed in Tables S3 and S4. Atomic coordinates are collected in Tables S5 and S6. Final Rietveld refinement fits are shown in Figures S9-S12.

#### Small Angle X-ray Scattering

Small angle X-ray scattering (SAXS) experiments were performed on a SAXSLAB Ganesha equipped with a Xenocs GeniX3D Cu K $\alpha$  source. SAXS samples were loaded into 1.0 mm OD x 0.01 mm wall borosilicate glass tubes and sealed under N<sub>2</sub> with wax. A near-saturated solution of **2** in dry DMF (approx. 2 mg/mL) was prepared and passed through a 0.2  $\mu\text{m}$  PET syringe filter prior to loading into the tube. A tube with neat DMF was used as the blank. SAXS data were collected in six 1-hour increments and compared to check for radiation damage, which was not found. All experiments were performed at

ambient temperature. Data reduction/integration was performed using Saxsgui software, and background subtraction and fitting were performed in the Irena software suite.<sup>16c</sup> Linear fits were performed in OriginPro software. Data were also fit using the Unified Fit module in Irena, based on the work of Beaucage.<sup>16</sup>

#### Optical Spectroscopy

UV-visible absorption spectra were recorded on a Thermo Scientific Evolution 300 spectrometer with the VISIONpro software suite. All spectra were recorded at room temperature. Diffuse reflectance spectra were obtained with the use of a Harrick Praying Mantis accessory. Solid **1** or **2** was ground with [Mg][SO<sub>4</sub>] in air to produce the diffuse reflectance sample and pure [Mg][SO<sub>4</sub>] was used as a white reference material. All spectra were normalized and had a background subtraction applied.

#### X-ray Photoelectron Spectroscopy

X-ray photoelectron spectra (XPS) were collected with the AXIS Nova spectrometer (Kratos Analytical) equipped with a monochromatic Al K $\alpha$  X-ray source. The Al anode was powered at 10 mA and 15 kV. The instrument work function was calibrated to give an Au 4f<sub>7/2</sub> metallic gold binding energy of 83.95 eV. Instrument base pressure was ca. 1 $\times$ 10<sup>-10</sup> Torr. The analysis area size was 0.3 x 0.7 mm<sup>2</sup>. For calibration purposes, the binding energies were referenced to C 1s peak at 284.8 eV. Survey spectra were collected with a step size of 1 eV and 160 eV pass energy. The high-resolution spectra were collected with a pass energy of 40 eV and 0.1 eV step size. Powder samples were affixed to conductive carbon tape in air before loading into the spectrometer.

For **1**, Fe, S, N, C, and O (likely from atmospheric adsorbates) are present. Quantification results provide the molar ratio of Fe:S:N = 1:1.96:0.52. For **2**, Fe, S, N, C, and O are again detected. Only Fe and S could be quantified, giving a molar ratio Fe:S = 1:1.95. For both **1** and **2**, XPS seems consistent with mixed valent Fe in the Fe<sup>2+/3+</sup> state; C 1s shows C-C/C-H and C-N bonds (indicated by broadening at about 286 eV); the S 2p<sub>3/2</sub> shift of 161.5 eV corresponds to S<sup>2-</sup> as in a sulfide ion or organic thiols – these species have close shifts and closely overlap. The N 1s spectrum appears as a sharp single peak located at 401.8 eV that fits well with reported binding energies of alkyl ammonium salts.<sup>41</sup> Li 1s overlaps with Fe 3p so it is difficult to assess Li content by XPS.

#### Mössbauer Spectroscopy

<sup>57</sup>Fe Mössbauer spectra were measured at 80 K, 25 K, or 4.2 K with zero applied magnetic field, using a constant acceleration spectrometer with a <sup>57</sup>Co on Rh source. Samples were encased in Paratone-N oil and placed in a polyethylene sample cup inside a N<sub>2</sub>-filled glovebox. Samples were frozen in liquid N<sub>2</sub> immediately upon removal from the glovebox and kept cold while loading into the spectrometer. Spectra were analyzed using WMOSS software. The sample of reduced, air-exposed **2** was prepared by exposing the reduced **2** Mössbauer sample to dry air (passed over P<sub>2</sub>O<sub>5</sub>) for 15 minutes.

#### Infrared Spectroscopy

Infrared spectra were recorded on a Bruker Tensor II FTIR spectrometer with MCT detector operated at 77 K. Data were processed and background corrected with OPUS software (version 7.5). An additional manual correction for scattering was also applied. Samples were prepared under N<sub>2</sub> by grinding

solid **1** or **2** with Nujol, placed between two KBr crystal plates, and measured in air under ambient conditions.

### Electrochemical Measurements

Electrical conductivity measurements were performed in a two-contact geometry at room temperature under N<sub>2</sub>. Samples were prepared as pressed pellets clamped between two brass electrodes (4.8 mm diam.) in a plastic sleeve, allowing measurement of the sample thickness with calipers. Linear sweep voltammetry was conducted using a BASi Epsilon potentiostat/galvanostat, with the reference and counter electrode terminals connected to one electrode and the working electrode terminal to the other. The resulting data were fit to a straight line to obtain the sample resistance. All values have been measured in triplicate on separate batches.

Electrochemical experiments were performed using cyclic voltammetry (CV) or differential pulse voltammetry (DPV) on a BASi Epsilon potentiostat/galvanostat. A glassy carbon working electrode, platinum wire counter electrode, and silver wire pseudoreference electrode were used for all measurements. Due to overlap of the irreversible [Fe<sub>4</sub>S<sub>4</sub>]<sup>2+</sup> oxidation with the FeCp<sub>2</sub><sup>+</sup>/FeCp<sub>2</sub> couple, CoCp<sub>2</sub> was used as an internal standard, and the CoCp<sub>2</sub><sup>+</sup>/CoCp<sub>2</sub> and CoCp<sub>2</sub>/CoCp<sub>2</sub><sup>-</sup> couples were referenced to FeCp<sub>2</sub><sup>+</sup>/FeCp<sub>2</sub> in a separate electrolyte solution under the same conditions. Unless otherwise noted, all scans were performed with a reductive initial scan direction.

### ASSOCIATED CONTENT

Analytical data and additional spectra and electrochemistry data. This material is available free of charge via the Internet at <http://pubs.acs.org>.

### AUTHOR INFORMATION

#### Corresponding Author

\*jsanderson@uchicago.edu

#### Author Contributions

‡These authors contributed equally. The manuscript was written through contributions of all authors. All authors have given approval to the final version of the manuscript.

#### Notes

The authors declare no competing financial interest.

### ACKNOWLEDGMENT

We thank Dr. Jordan DeGayner and Prof. T. David Harris for assistance with Mössbauer spectroscopy. We thank Wenbo Han and Prof. Wenbin Lin for assistance with ICP-MS measurements. We thank Vlad Kamysbayev and Prof. Dmitri Talapin for assistance with ICP-OES measurements. This work was supported by the U. S. Department of Energy, Office of Science, Office of Basic Energy Sciences, under Award No. DE-SC0019215. This work was supported by the Chicago MRSEC, which is funded by NSF through Grant DMR-1420709. The University of Chicago is thanked for startup funds. Use of the Advanced Photon Source at Argonne National Laboratory was supported by the U. S. Department of Energy, Office of Science, Office of Basic Energy Sciences, under Contract No. DE-AC02-06CH11357, and we thank the 11-BM beamline staff. SOLEIL Synchrotron beamtime at the PROXIMA 2A beamline is gratefully acknowledged. Mia Grahn was supported by a partnership between the Institute for Molecular Engineering and After School Matters. Chloe Gilder was supported through the NSF by an NSF CAREER award Grant No. 1654144 to John S. Anderson.

### REFERENCES

- (1) (a) Li, J. R.; Kuppler, R. J.; Zhou, H. C. Selective Gas Adsorption and Separation in Metal-Organic Frameworks. *Chem. Soc. Rev.* **2009**, *38* (5), 1477–1504. (b) Lee, J.; Farha, O. K.; Roberts, J.; Scheidt, K. A.; Nguyen, S. T.; Hupp, J. T. Metal-Organic Framework Materials as Catalysts. *Chem. Soc. Rev.* **2009**, *38* (5), 1450–1459. (c) Ma, L.; Abney, C.; Lin, W. Enantioselective Catalysis with Homochiral Metal-Organic Frameworks. *Chem. Soc. Rev.* **2009**, *38* (5), 1248. (d) Sumida, K.; Rogow, D. L.; Mason, J. A.; McDonald, T. M.; Bloch, E. D.; Herm, Z. R.; Bae, T.-H.; Long, J. R. Carbon Dioxide Capture in Metal-Organic Frameworks. *Chem. Rev.* **2012**, *112* (2), 724–781. (e) Furukawa, H.; Cordova, K. E.; O’Keeffe, M.; Yaghi, O. M. The Chemistry and Applications of Metal-Organic Frameworks. *Science* (80). **2013**, *341* (6149), 1230444–1230444. (f) Zhang, Y.; Feng, X.; Yuan, S.; Zhou, J.; Wang, B. Challenges and Recent Advances in MOF-Polymer Composite Membranes for Gas Separation. *Inorg. Chem. Front.* **2016**, *3* (7), 896–909. (g) Maurin, G.; Serre, C.; Cooper, A.; Férey, G. The New Age of MOFs and of Their Porous-Related Solids. *Chem. Soc. Rev.* **2017**, *46* (11), 3104–3107. (h) Trickett, C. A.; Helal, A.; Al-Maythaly, B. A.; Yamani, Z. H.; Cordova, K. E.; Yaghi, O. M. The Chemistry of Metal-Organic Frameworks for CO<sub>2</sub> Capture, Regeneration and Conversion. *Nat. Rev. Mater.* **2017**, *2* (8), 17045.
- (2) (a) Kojima, A.; Teshima, K.; Shirai, Y.; Miyasaka, T., Organometal Halide Perovskites as Visible-Light Sensitizers for Photovoltaic Cells. *J. Am. Chem. Soc.* **2009**, *131* (17), 6050–6051. (b) Hao, F.; Stoumpos, C. C.; Cao, D. H.; Chang, R. P. H.; Kanatzidis, M. G., Lead-Free Solid-State Organic-Inorganic Halide Perovskite Solar Cells. *Nat. Photonics* **2014**, *8*, 489. (c) Zhao, Y.; Zhu, K., Organic-Inorganic Hybrid Lead Halide Perovskites for Optoelectronic and Electronic Applications. *Chem. Soc. Rev.* **2016**, *45* (3), 655–689. (d) Slavney, A. H.; Hu, T.; Lindenberg, A. M.; Karunadasa, H. I. A Bismuth-Halide Double Perovskite with Long Carrier Recombination Lifetime for Photovoltaic Applications. *J. Am. Chem. Soc.* **2016**, *138*, 2138–2141. (e) Smith, M. D.; Karunadasa, H. I. White-Light Emission from Layered Halide Perovskites. *Acc. Chem. Res.* **2018**, *51*, 619–627.
- (3) (a) Bhattacharya, B.; Layek, A.; Mehboob Alam, M.; Maity, D. K.; Chakrabarti, S.; Ray, P. P.; Ghoshal, D. Cd(II) Based Metal-Organic Framework Behaving as a Schottky Barrier Diode. *Chem. Commun.* **2014**, *50* (58), 7858. (b) Sheberla, D.; Sun, L.; Blood-Forsythe, M. A.; Er, S.; Wade, C. R.; Brozek, C. K.; Aspuru-Guzik, A.; Dincă, M. High Electrical Conductivity in Ni<sub>3</sub>(2,3,6,7,10,11-Hexamino)triphenylene)<sub>2</sub>, a Semiconducting Metal-Organic Graphene Analogue. *J. Am. Chem. Soc.* **2014**, *136* (25), 8859–8862. (c) Campbell, M. G.; Sheberla, D.; Liu, S. F.; Swager, T. M.; Dincă, M. Cu<sub>3</sub>(Hexamino)triphenylene)<sub>2</sub>: an Electrically Conductive 2D Metal-Organic Framework for Chemiresistive Sensing. *Angew. Chem., Int. Ed.* **2015**, *54* (14), 4349–4352. (d) Darago, L. E.; Aubrey, M. L.; Yu, C. J.; Gonzalez, M. I.; Long, J. R. Electronic Conductivity, Ferrimagnetic Ordering, and Reductive Insertion Mediated by Organic Mixed-Valence in a Ferric Semiquinoid Metal-Organic Framework. *J. Am. Chem. Soc.* **2015**, *137* (50), 15703–15711. (e) Jeon, I.-R.; Negru, B.; Van Duyne, R. P.; Harris, T. D. A 2D Semiquinone Radical-Containing Microporous Magnet with Solvent-Induced Switching from T<sub>c</sub> = 26 To 80 K. *J. Am. Chem. Soc.* **2015**, *137* (50), 15699–15702. (f) Wang, L.; Han, Y.; Feng, X.; Zhou, J.; Qi, P.; Wang, B. Metal-Organic Frameworks for Energy Storage: Batteries and Supercapacitors. *Coord. Chem. Rev.* **2016**, *307*, 361–381. (g) Shi, C.; Xia, Q.; Xue, X.; Liu, Q.; Liu, H. J. Synthesis of Cobalt-Based Layered Coordination Polymer Nanosheets and Their Application in Lithium-Ion Batteries as Anode Materials. *RSC Adv.* **2016**, *6* (6), 4442–4447. (h) Liu, W.; Yin, X.-B. Metal-Organic Frameworks for Electrochemical Applications. *Trends Anal. Chem.* **2016**, *75*, 86–96. (i) Jeon, I.-R.; Sun, L.; Negru, B.; Van Duyne, R. P.; Dincă, M.; Harris, T. D. Solid-State Redox Switching of Magnetic Exchange and Electronic Conductivity in a Benzoquinoid-Bridged Mn II Chain Compound. *J. Am. Chem. Soc.* **2016**, *138* (20), 6583–6590. (j) Degayner, J. A.; Jeon, I. R.; Sun, L.; Dincă, M.; Harris, T. D. 2D Conductive Iron-Quinoid Magnets Ordering up to T<sub>c</sub> = 105 K via Heterogeneous Redox Chemistry. *J. Am. Chem. Soc.* **2017**, *139* (11), 4175–4184. (k) Dou, J.-H.; Sun, L.; Ge, Y.; Li, W.; Hendon, C. H.; Li, J.; Gul, S.; Yano, J.; Stach, E. A.; Dincă, M. Signature of Metallic Behavior in the Metal-Organic Frameworks M<sub>3</sub>(Hexamino)benzene)<sub>2</sub> (M = Ni, Cu). *J. Am. Chem. Soc.* **2017**, *139* (39), 13608–13611. (l) Sheberla, D.; Bachman, J. C.; Elias, J. S.; Sun, C.-J.; Shao-Horn, Y.; Dincă, M. Conductive MOF Electrodes for Stable Supercapacitors with High Areal Capacitance. *Nat. Mater.* **2017**,

- 16 (2), 220–224. (m) Sun, L.; Liao, B.; Sheberla, D.; Kraemer, D.; Zhou, J.; Stach, E. A.; Zakharov, D.; Stavila, V.; Talin, A. A.; Ge, Y.; Allendorff, M. D.; Chen, G.; Léonard, F.; Dincă, M. A Microporous and Naturally Nanostructured Thermoelectric Metal–Organic Framework with Ultralow Thermal Conductivity. *Joule* **2017**, *1* (1), 168–177. (n) Wada, K.; Sakaushi, K.; Sasaki, S.; Nishihara, H. Multielectron-Transfer-Based Rechargeable Energy Storage of Two-Dimensional Coordination Frameworks with Non-Innocent Ligands. *Angew. Chem., Int. Ed.* **2018**, *57* (29), 8886–8890. (o) Park, J.; Lee, M.; Feng, D.; Huang, Z.; Hinckley, A. C.; Yakovenko, A.; Zou, X.; Cui, Y.; Bao, Z. Stabilization of Hexaaminobenzene in a 2D Conductive Metal–Organic Framework for High Power Sodium Storage. *J. Am. Chem. Soc.* **2018**, *140* (32), 10315–10323. (p) Feng, D.; Lei, T.; Lukatskaya, M. R.; Park, J.; Huang, Z.; Lee, M.; Shaw, L.; Chen, S.; Yakovenko, A. A.; Kulkarni, A.; Xiao, J.; Fredrickson, K.; Tok, J. B.; Zou, X.; Cui, Y.; Bao, Z. Robust and Conductive Two-Dimensional Metal–Organic Frameworks with Exceptionally High Volumetric and Areal Capacitance. *Nat. Energy* **2018**, *3* (1), 30–36. (q) Ziebel, M. E.; Darago, L. E.; Long, J. R. Control of Electronic Structure and Conductivity in Two-Dimensional Metal–Semiquinoid Frameworks of Titanium, Vanadium, and Chromium. *J. Am. Chem. Soc.* **2018**, *140* (8), 3040–3051. (r) Aubrey, M. L.; Wiers, B. M.; Andrews, S. C.; Sakurai, T.; Reyes-Lillo, S. E.; Hamed, S. M.; Yu, C.; Darago, L. E.; Mason, J. A.; Baeg, J.; Grandjean, F.; Long, G. J.; Seki, S.; Neaton, J. B.; Yang, P.; Long, J. R. Electron Delocalization and Charge Mobility as a Function of Reduction in a Metal–Organic Framework. *Nat. Mater.* **2018**, *17* (7), 625–632. (s) Xie, L. S.; Sun, L.; Wan, R.; Park, S. S.; Degayner, J. A.; Hendon, C. H.; Dincă, M. Tunable Mixed-Valence Doping Toward Record Electrical Conductivity in a Three-Dimensional Metal–Organic Framework. *J. Am. Chem. Soc.* **2018**, *140* (24), 7411–7414.
- (4) (a) Fourmigué, M.; Uzelmeier, C. E.; Boubekeur, K.; Bartley, S. L.; Dunbar, K. R. Bis- and Tetrakis(Diphenylphosphino) Tetrathiafulvalenes as Precursors of Redox-Active Organic–Inorganic Polymeric Networks. *J. Organomet. Chem.* **1997**, *529*, 343–350. (b) Smucker, B. W.; Dunbar, K. R. Homoleptic Complexes of Ag(I), Cu(I), Pd(II) and Pt(II) with Tetrathiafulvalene-Functionalized Phosphine Ligands. *J. Chem. Soc. Dalton* **2000**, 1309–1315. (c) Sun, Y.; Sheng, P.; Di, C.; Jiao, F.; Xu, W.; Qiu, D.; Zhu, D. Organic Thermoelectric Materials and Devices Based on P- and N-Type Poly(Metal 1,1,2,2-Ethenetetra-thiolate)S. *Adv. Mater.* **2012**, *24* (7), 932–937. (d) Givajva, G.; Amo-Ochoa, P.; Gómez-García, C. J.; Zamora, F. Electrical Conductive Coordination Polymers. *Chem. Soc. Rev.* **2012**, *41* (1), 115–147. (e) Sun, L.; Miyakai, T.; Seki, S.; Dincă, M. Mn<sub>2</sub>(2,5-Disulfhydrylbenzene-1,4-Dicarboxylate): a Microporous Metal–Organic Framework with Infinite (–Mn–S–)∞ Chains and High Intrinsic Charge Mobility. *J. Am. Chem. Soc.* **2013**, *135* (22), 8185–8188. (f) Sun, L.; Hendon, C. H.; Minier, M. A.; Walsh, A.; Dincă, M. Million-Fold Electrical Conductivity Enhancement in Fe<sub>2</sub>(DEBDC) versus Mn<sub>2</sub>(DEBDC) (E = S, O). *J. Am. Chem. Soc.* **2015**, *137* (19), 6164–6167. (g) Sun, Y.; Qiu, L.; Tang, L.; Geng, H.; Wang, H.; Zhang, F.; Huang, D.; Xu, W.; Yue, P.; Guan, Y. S.; Jiao, F.; Sun, Y.; Tang, D.; Di, C.; Yi, Y.; Zhu, D. Flexible N-Type High-Performance Thermoelectric Thin Films of Poly(Nickel-Ethylenetetra-thiolate) Prepared by an Electrochemical Method. *Adv. Mater.* **2016**, *28* (17), 3351–3358. (h) Sun, L.; Campbell, M. G.; Dincă, M. Electrically Conductive Porous Metal–Organic Frameworks. *Angew. Chem., Int. Ed.* **2016**, *55* (11), 3566–3579.
- (5) (a) Rivera, N. M.; Engler, E. M.; Schumaker, R. R. Synthesis and Properties of Tetrathiafulvalene–Metal Bis(dithiolene) Macromolecules. *J. Chem. Soc., Chem. Commun.* **1979**, 4, 184–185. (b) Dirk, C. W.; Bousseau, M.; Barrett, P. H.; Moraes, F.; Wudl, F.; Heeger, A. J. Metal Poly(Benzodithiolenes). *Macromolecules* **1986**, *19* (2), 266–269. (c) Vicente, R.; Ribas, J.; Cassoux, P.; Valade, L. Synthesis, Characterization and Properties of Highly Conducting Organometallic Polymers Derived from the Ethylene Tetrathiolate Anion. *Synth. Met.* **1986**, *13* (4), 265–280. (d) Szczepura, L. F.; Galloway, C. P.; Zheng, Y.; Han, P.; Wilson, S. R.; Rauchfuss, T. B.; Rheingold, A. L. C<sub>4</sub>S<sub>6</sub><sup>2-</sup>: a Bridging Bis(Dithiolato) Ligand for the Preparation of Semiconducting Inorganic Polymers. *Angew. Chem., Int. Ed.* **1995**, *34* (17), 1890–1892. (e) Cerrada, E.; Diaz, M. C.; Diaz, C.; Laguna, M.; Sabater, A. New Conducting Coordination Polymers Containing M(Dmit)<sub>2</sub> Links. *Synth. Met.* **2001**, *119* (1–3), 91–92. (f) Mitsumi, M.; Murase, T.; Kishida, H.; Yoshinari, T.; Ozawa, Y.; Toriumi, K.; Sonoyama, T.; Kitagawa, H.; Mitani, T. Metallic Behavior and Periodical Valence Ordering in a MMX Chain Compound, Pt<sub>2</sub>(EtCS<sub>2</sub>)<sub>4</sub>. *J. Am. Chem. Soc.* **2001**, *123* (45), 11179–11192. (g) Kanehama, R.; Umemiya, M.; Iwahori, F.; Miyasaka, H.; Sugiura, K.; Yamashita, M.; Yokochi, Y.; Ito, H.; Kuroda, S.; Kishida, H.; Okamoto, H. Novel ET-Coordinated Copper(I) Complexes: Syntheses, Structures, and Physical Properties (ET = BEDT-TTF = Bis(Ethylenedithio)Tetrathiafulvalene). *Inorg. Chem.* **2003**, *42* (22), 7173–7181.
- (6) (a) Kambe, T.; Sakamoto, R.; Hoshiko, K.; Takada, K.; Miyachi, M.; Ryu, J. H.; Sasaki, S.; Kim, J.; Nakazato, K.; Takata, M.; Nishihara, H. A π-Conjugated Nickel Bis(Dithiolene) Complex Nanosheet. *J. Am. Chem. Soc.* **2013**, *135* (7), 2462–2465. (b) Kambe, T.; Sakamoto, R.; Kusamoto, T.; Pal, T.; Fukui, N.; Hoshiko, K.; Shimojima, T.; Wang, Z.; Hirahara, T.; Ishizaka, K.; Hasegawa, S.; Liu, F.; Nishihara, H. Redox Control and High Conductivity of Nickel Bis(Dithiolene) Complex π-Nanosheet: a Potential Organic Two-Dimensional Topological Insulator. *J. Am. Chem. Soc.* **2014**, *136* (41), 14357–14360. (c) Huang, X.; Sheng, P.; Tu, Z.; Zhang, F.; Wang, J.; Geng, H.; Zou, Y.; Di, C.; Yi, Y.; Sun, Y.; Xu, W.; Zhu, D. A Two-Dimensional π-d Conjugated Coordination Polymer with Extremely High Electrical Conductivity and Ambipolar Transport Behaviour. *Nat. Commun.* **2015**, *6* (1), 7408. (d) Dong, R.; Pfeiffermann, M.; Liang, H.; Zheng, Z.; Zhu, X.; Zhang, J.; Feng, X. Large-Area, Free-Standing, Two-Dimensional Supramolecular Polymer Single-Layer Sheets for Highly Efficient Electrochemical Hydrogen Evolution. *Angew. Chem., Int. Ed.* **2015**, *54* (41), 12058–12063. (e) Pal, T.; Kambe, T.; Kusamoto, T.; Foo, M. L.; Matsuoka, R.; Sakamoto, R.; Nishihara, H. Interfacial Synthesis of Electrically Conducting Palladium Bis(Dithiolene) Complex Nanosheet. *Chempluschem* **2015**, *80* (8), 1255–1258. (f) Clough, A. J.; Yoo, J. W.; Mecklenburg, M. H.; Marinescu, S. C. Two-Dimensional Metal–Organic Surfaces for Efficient Hydrogen Evolution from Water. *J. Am. Chem. Soc.* **2015**, *137* (1), 118–121. (g) Maeda, H.; Sakamoto, R.; Nishihara, H. Coordination Programming of Two-Dimensional Metal Complex Frameworks. *Langmuir* **2016**, *32* (11), 2527–2538. (h) Huang, X.; Yao, H.; Cui, Y.; Hao, W.; Zhu, J.; Xu, W.; Zhu, D. Conductive Copper Benzenehexathiol Coordination Polymer as a Hydrogen Evolution Catalyst. *ACS Appl. Mater. Interfaces* **2017**, *9* (46), 40752–40759. (i) Huang, X.; Zhang, S.; Liu, L.; Yu, L.; Chen, G.; Xu, W.; Zhu, D. Superconductivity in a Copper(II)-Based Coordination Polymer with Perfect Kagome Structure. *Angew. Chem., Int. Ed.* **2018**, *57* (1), 146–150.
- (7) Ji, Z.; Trickett, C.; Pei, X.; Yaghi, O. M., Linking Molybdenum–Sulfur Clusters for Electrocatalytic Hydrogen Evolution. *J. Am. Chem. Soc.* **2018**, Article ASAP, DOI:10.1021/jacs.8b09807
- (8) (a) Beinert, H.; Holm, R. H.; Münck, E., Iron-Sulfur Clusters: Nature’s Modular, Multipurpose Structures. *Science* **1997**, *277* (5326), 653–659. (b) Venkateswara Rao, P.; Holm, R. H., Synthetic Analogues of the Active Sites of Iron–Sulfur Proteins. *Chem. Rev.* **2004**, *104* (2), 527–560. (c) McSkimming, A.; Suess, D. L. M. Selective Synthesis of Site-Differentiated Fe<sub>4</sub>S<sub>4</sub> and Fe<sub>6</sub>S<sub>6</sub> Clusters. *Inorg. Chem.* **2018**, *57*, 14904–14912.
- (9) (a) Jormakka, M.; Törnroth, S.; Byrne, B.; Iwata, S., Molecular Basis of Proton Motive Force Generation: Structure of Formate Dehydrogenase-N. *Science* **2002**, *295* (5561), 1863–1868. (b) Jormakka, M.; Richardson, D.; Byrne, B.; Iwata, S., Architecture of NarGH Reveals a Structural Classification of Mo-bisMGD Enzymes. *Structure* **2004**, *12* (1), 95–104. (c) Sazanov, L. A.; Hincliffe, P., Structure of the Hydrophilic Domain of Respiratory Complex I from *Thermus thermophilus*. *Science* **2006**, *311* (5766), 1430–1436. (d) Jormakka, M.; Yokoyama, K.; Yano, T.; Tamakoshi, M.; Akimoto, S.; Shimamura, T.; Curmi, P.; Iwata, S., Molecular Mechanism of Energy Conservation in Polysulfide Respiration. *Nat. Struct. Mol. Biol.* **2008**, *15*, 730. (e) Hayashi, T.; Stuchebrukhov, A. A., Electron Tunneling in Respiratory Complex I. *Proc. Natl. Acad. Sci. U.S.A.* **2010**, *107* (45), 19157–19162. (f) Weinert, T.; Huwiler, S. G.; Kung, J. W.; Weidenweber, S.; Hellwig, P.; Stärk, H.-J.; Biskup, T.; Weber, S.; Cotelesage, J. J. H.; George, G. N.; Ermiler, U.; Boll, M., Structural Basis of Enzymatic Benzene Ring Reduction. *Nat. Chem. Biol.* **2015**, *11*, 586. (g) Youngblut, M. D.; Tsai, C.-L.; Clark, I. C.; Carlson, H. K.; Maglaqui, A. P.; Gau-Pan, P. S.; Redford, S. A.; Wong, A.; Tainer, J. A.; Coates, J. D., Perchlorate Reductase is Distinguished by Active Site Aromatic Gate Residues. *J. Biol. Chem.* **2016**, *291* (17), 9190–9202. (h) Wagner, T.; Ermiler, U.; Shima, S., The Methanogenic CO<sub>2</sub> Reducing-and-Fixing Enzyme is Bifunctional and Contains 46 [4Fe–4S] clusters. *Science* **2016**, *354* (6308), 114–117. (i) Glasser, N. R.; Oyala, P. H.; Osborne, T. H.; Santini, J. M.; Newman, D. K., Structural and Mechanistic Analysis of the Arsenate Respiratory Reductase Provides Insight into Environmental Arsenic Transformations. *Proc. Natl. Acad. Sci. U.S.A.* **2018**, published ahead of print August 13, 2018 <https://doi.org/10.1073/pnas.1807984115>.
- (10) Trikalitis, P. N.; Bakas, T.; Papaefthymiou, V.; Kanatzidis, M. G., Supramolecular Assembly of Hexagonal Mesostructured Germanium

- Sulfide and Selenide Nanocomposites Incorporating the Biologically Relevant  $\text{Fe}_4\text{S}_4$  Cluster. *Angew. Chem., Int. Ed.* **2000**, *39* (24), 4558-4562.
- (11) (a) Yuhas, B. D.; Prasittichai, C.; Hupp, J. T.; Kanatzidis, M. G., Enhanced Electrocatalytic Reduction of  $\text{CO}_2$  with Ternary Ni- $\text{Fe}_4\text{S}_4$  and Co- $\text{Fe}_4\text{S}_4$ -Based Biomimetic Chalcogels. *J. Am. Chem. Soc.* **2011**, *133* (40), 15854-15857. (b) Shim, Y.; Yuhas, B. D.; Dyar, S. M.; Smeigh, A. L.; Douvalis, A. P.; Wasielewski, M. R.; Kanatzidis, M. G., Tunable Biomimetic Chalcogels with  $\text{Fe}_4\text{S}_4$  Cores and  $[\text{Sn}_n\text{S}_{2n+2}]^{4-}$  ( $n = 1, 2, 4$ ) Building Blocks for Solar Fuel Catalysis. *J. Am. Chem. Soc.* **2013**, *135* (6), 2330-2337.
- (12) (a) Moutet, J.-C.; Pickett, C. J., Iron-Sulphur Clusters in Ionic Polymers on Electrodes. *J. Chem. Soc., Chem. Commun.* **1989**, 3, 188-190. (b) Pickett, C. J.; Ryder, K. S.; Moutet, J.-C., Synthesis and Anodic Polymerisation of an L-Cystine Derivatised Pyrrole; Copolymerisation with a Tetraalkylammonium Pyrrole Allows Reduction of the Cystinyl Film to a Cysteinyll State that Binds Electroactive  $[\text{Fe}_4\text{S}_4]^{2+}$  Centres. *J. Chem. Soc., Chem. Commun.* **1992**, 9, 694-697. (c) Pickett, C. J.; Ryder, K. S.; Moutet, J.-C., Iron-Sulfur Clusters in Ionic Polymers on Electrodes. *J. Chem. Soc., Dalton Trans.* **1993**, 24, 3695-3703. (d) Pickett, C. J.; Ryder, K. S., Bioinorganic Reaction Centres on Electrodes. Modified Electrodes Possessing Amino Acid, Peptide and Ferredoxin-Type Groups on a Poly(pyrrole) Backbone. *J. Chem. Soc., Dalton Trans.* **1994**, 14, 2181-2189.
- (13) Rancourt, D. G.; Ping, J. Y., Voigt-Based Methods for Arbitrary-Shape Static Hyperfine Parameter Distributions in Mössbauer Spectroscopy. *Nucl. Instrum. Methods Phys. Res.* **1991**, *58* (1), 85-97.
- (14) (a) Morris, W.; Wang, S.; Cho D.; Auyeung, E.; Li, P.; Farha, O. K.; Mirkin, C. A. Role of Modulators in Controlling the Colloidal Stability and Polydispersity of the UiO-66 Metal-Organic Framework. *ACS Appl. Mater. Interfaces* **2017**, *9*, 33413-33418. (b) Schaate, A.; Roy, P.; Godt, A.; Lippke, J.; Waltz, F.; Wiebecke, M.; Behrens, P. Modulated Synthesis of Zr-Based Metal-Organic Frameworks: From Nano to Single Crystals. *Chem. Eur. J.* **2011**, *17*, 6643 - 6651.
- (15) Friese, V. A. and Kurth, D. G. Soluble dynamic coordination polymers as a paradigm for materials science. *Coord. Chem. Rev.* **2008**, *252*, 199-211.
- (16) (a) Beaucage, G., Approximations Leading to a Unified Exponential/Power-Law Approach to Small-Angle Scattering. *J. Appl. Crystallogr.* **1995**, *28* (6), 717-728. (b) Beaucage, G., Small-Angle Scattering from Polymeric Mass Fractals of Arbitrary Mass-Fractal Dimension. *J. Appl. Crystallogr.* **1996**, *29* (2), 134-146. (c) Ilavsky, J.; Jemian, P. R., Irena: Tool Suite for Modeling and Analysis of Small-Angle Scattering. *J. Appl. Crystallogr.* **2009**, *42* (2), 347-353.
- (17) Hammouda, B.; Worcester, D., The Denaturation Transition of DNA In Mixed Solvents. *Biophys. J.* **2006**, *91* (6), 2237-2242.
- (18) Page, C. C.; Moser, C. C.; Chen, X.; Dutton, P. L., Natural Engineering Principles of Electron Tunnelling in Biological Oxidation-Reduction. *Nature* **1999**, *402*, 47.
- (19) Depamphilis, B. V.; Averill, B. A.; Herskovitz, T.; Que, L.; Holm, R. H., Synthetic Analogs of the Active Sites of Iron-Sulfur Proteins. VI. Spectral and Redox Characteristics of the Tetranuclear Clusters  $[\text{Fe}_4\text{S}_4(\text{SR})_4]^{2-}$ . *J. Am. Chem. Soc.* **1974**, *96* (13), 4159-4167.
- (20) Venkateswara Rao, P.; Holm, R. H., Synthetic Analogues of the Active Sites of Iron-Sulfur Proteins. *Chem. Rev.* **2004**, *104* (2), 527-560.
- (21) O'Sullivan, T.; Millar, M. M., Synthesis and Study of An Analog for the  $[\text{Fe}_4\text{S}_4]^{3+}$  Center of Oxidized High Potential Iron-Sulfur Proteins. *J. Am. Chem. Soc.* **1985**, *107* (13), 4096-4097.
- (22) Sun, L.; Park, S. S.; Sheberla, D.; Dincă, M. Measuring and Reporting Electrical Conductivity in Metal-Organic Frameworks:  $\text{Cd}_2(\text{TTFTB})$  as a Case Study. *J. Am. Chem. Soc.* **2016**, *138* (44), 14772-14782.
- (23) Laskowski, E. J.; Frankel, R. B.; Gillum, W. O.; Papaefthymiou, G. C.; Renaud, J.; Ibers, J. A.; Holm, R. H., Synthetic Analogs of the 4-Fe Active Sites of Reduced Ferredoxins. Electronic Properties of the Tetranuclear Trianions  $[\text{Fe}_4\text{S}_4(\text{SR})_4]^{3-}$  and the structure of  $[(\text{C}_6\text{H}_5)_3(\text{CH}_3)\text{N}]_3[\text{Fe}_4\text{S}_4(\text{SC}_6\text{H}_5)_4]$ . *J. Am. Chem. Soc.* **1978**, *100* (17), 5322-5337.
- (24) Kanatzidis, M. G.; Baenziger, N. C.; Coucouvanis, D.; Simopoulos, A.; Kostikas, A., Synthesis, Structural Characterization, and Electronic Structures of the Mixed Terminal Ligand Iron-Sulfur Cubanes  $[\text{Fe}_4\text{S}_4\text{Cl}_2(\text{XPh})_2]^{2-}$  ( $\text{X} = \text{S}, \text{O}$ ) and  $[\text{Fe}_4\text{S}_4(\text{SPh})_2(\text{OC}_6\text{H}_4\text{Me-p})_2]^{2-}$ . The First Examples of  $[\text{Fe}_4\text{S}_4]^{2+}$  Cores With a Noncompressed  $D_{2d}$  Idealized Geometry. *J. Am. Chem. Soc.* **1984**, *106* (16), 4500-4511.
- (25) Cambray, J.; Lane, R. W.; Wedd, A. G.; Johnson, R. W.; Holm, R. H., Chemical and Electrochemical Interrelationships of the 1-Fe, 2-Fe, and 4-Fe Analogs of the Active Sites of Iron-Sulfur Proteins. *Inorg. Chem.* **1977**, *16* (10), 2565-2571.
- (26) Willy, L.; Emil, M., Über die Salze der Phosphor-Hexafluorwasserstoffsäure,  $\text{HPF}_6$ . *Ber. Dtsch. Chem. Ges. (A And B Series)* **1930**, *63* (5), 1058-1070.
- (27) Christou, G.; Garner, C. D.; Balasubramanian, A.; Ridge, B.; Rydon, H. N.; Stiefel, E. I.; Pan, W.-H., Tetranuclear Iron-Sulfur and Iron-Selenium Clusters. In *Inorg. Synth.*, Fackler, J. P. J., Ed. 1982; Vol. 21.
- (28) Maiolo, F.; Testaferri, L.; Tiecco, M.; Tingoli, M., Fragmentation of Aryl Alkyl Sulfides. A Simple, One-Pot Synthesis of Polymercaptobenzenes from Polychlorobenzenes. *J. Org. Chem.* **1981**, *46* (15), 3070-3073.
- (29) Que, L.; Bobrik, M. A.; Ibers, J. A.; Holm, R. H., Synthetic Analogs of the Active Sites of Iron-Sulfur Proteins. VII. Ligand Substitution Reactions of the Tetranuclear Clusters  $[\text{Fe}_4\text{S}_4(\text{SR})_2]^{2-}$  and the Structure of Bis(Tetramethylammonium)[Tetra- $\mu$ -Sulfide-Tetrakis(Benzenethiolato)Tetrairon]. *J. Am. Chem. Soc.* **1974**, *96* (13), 4168-4178.
- (30) Howarth, A. J.; Peters, A. W.; Vermeulen, N. A.; Wang, T. C.; Hupp, J. T.; Farha, O. K., Best Practices for the Synthesis, Activation, and Characterization of Metal-Organic Frameworks. *Chem. Mater.* **2017**, *29* (1), 26-39.
- (31) (a) <https://www.synchrotron-soleil.fr/fr/lignes-de-lumiere/proxima-2a> (b) Duran, D.; Le Couster, S.; Desjardins, K.; Delmotte, A.; Fox, G.; Meijers, R.; Moreno, T.; Savko, M.; Shepard, W., PROXIMA 2A - A New Fully Tunable Micro-Focus Beamline for Macromolecular Crystallography. *J. Phys.: Conf. Ser.* **2013**, *425*, 012005.
- (32) ALBULA (free) software (DECTRIS), <https://www.dectris.com/products/albula-software>.
- (33) Louër, D. and Boulitf, A., Some Further Considerations in Powder Diffraction Pattern Indexing with the Dichotomy Method. *Powder Diffr.* **2014**, *29* (Suppl. S2), S7-S12.
- (34) Altomare, A.; Giacovazzo, C.; Guagliardi, A.; Moliterni, A.; Rizzi, R.; Werner, P.-E., New Techniques for Indexing: N-TREOR in EXPO. *J. Appl. Crystallogr.* **2000**, *33*, 1180-1186.
- (35) PreDICT (free) software, International Centre for Diffraction Data, <http://www.icdd.com/index.php/predict/>.
- (36) Altomare, A.; Cuocci, C.; Giacovazzo, C.; Moliterni, A.; Rizzi, R.; Corriero, N.; Falcicchio, A., EXPO2013: a Kit of Tools for Phasing Crystal Structures from Powder Data. *J. Appl. Crystallogr.* **2013**, *46* (4), 1231-1235.
- (37) Favre-Nicolin, V.; Cerny, R.; FOX, 'Free Objects for Crystallography': a Modular Approach to ab initio Structure Determination from Powder Diffraction. *J. Appl. Crystallogr.* **2002**, *35* (6), 734-743.
- (38) Larson A. C. and Von Dreele, R. B., General Structure Analysis System (GSAS), Los Alamos National Laboratory Report LAUR **1994**, 86-748.
- (39) (a) Liu, Q.; Zhang, C.; Chen, C.; Zhu, H.; Deng, Y.; Cai, J., Syntheses and Structural Characterizations of  $\text{Fe}_4\text{S}_4$  Cubane-Like Cluster Compounds Containing Cycloalkylthiolate Ligands. *Sci. China Chem.* **1997**, *40* (6), 616-623. (b) Al-Rammahi, T. M. M.; Waddell, P. G.; Henderson, R. A. *CCDC 1472848: Experimental Crystal Structure Determination*, **2016**, DOI: 10.5517/ccdc.csd.cc11fm7w. (c) Al-Rammahi, T. M. M.; Waddell, P. G.; Henderson, R. A., X-ray Crystal Structures of  $[\text{NHR}_3]_2[\text{Fe}_4\text{S}_4\text{X}_4]$  ( $\text{X} = \text{PhS}, \text{R} = \text{Et}$  or  $n\text{Bu}$ ;  $\text{X} = \text{Cl}, \text{R} = n\text{Bu}$ ): Implications for Sites of Protonation in Fe-S Clusters. *Transition Met. Chem.* **2016**, *41* (5), 555-561.
- (40) <https://www.ccdc.cam.ac.uk/solutions/csd-system/components/mogul>.
- (41) (a) Macrae, C. F.; Edgington, P. R.; McCabe, P.; Pidcock, E.; Shields, G. P.; Taylor, R.; Towler, M.; van de Streek, J., Mercury: Visualization and Analysis of Crystal Structures. *J. Appl. Crystallogr.* **2006**, *39* (3), 453-457. (b) Macrae, C. F.; Bruno, I. J.; Chisholm, J. A.; Edgington, P. R.; McCabe, P.; Pidcock, E.; Rodriguez-Monge, L.; Taylor, R.; van de Streek, J.; Wood, P. A., Mercury CSD 2.0 - New Features for the Visualization and Investigation of Crystal Structures. *J. Appl. Crystallogr.* **2008**, *41* (2), 466-470.
- (42) <https://checkcif.iucr.org>.
- (43) Bhattacharyya, R.; Chakrabarty, P. K.; Ghosh, P. N.; Mukherjee, A. K.; Podder, D.; Mukherjee, M., Reaction of Tetraoxomolybdate(2-) and Tetraoxotungstate(2-) with Aqueous Polysulfides: Synthesis, Structure, and Electrochemistry of  $\eta^2$ -Polysulfido Complexes Containing a Bridging  $\text{S}_2\{\text{M}_2\text{O}_2\}^{2+}$  ( $\text{M} = \text{Molybdenum}, \text{Tungsten}$ ) Core. *Inorg. Chem.* **1991**, *30* (20), 3948-3955.

1  
2  
3  
4  
5  
6  
7  
8  
9  
10  
11  
12  
13  
14  
15  
16  
17  
18  
19  
20  
21  
22  
23  
24  
25  
26  
27  
28  
29  
30  
31  
32  
33  
34  
35  
36  
37  
38  
39  
40  
41  
42  
43  
44  
45  
46  
47  
48  
49  
50  
51  
52  
53  
54  
55  
56  
57  
58  
59  
60

## TOC

**Coordination Polymer Chains Built With  
Redox-Active Clusters**